# A Theoretical Study of Heterojunction and Graded Band Gap Type Solar Cells

Annual Report on
NASA Grant No.
NSG 1116

March 1976



J. R. Hauser and J. E. Sutherland

North Carolina State University
Electrical Engineering Department
Box 5275, Raleigh, NC 27607

# A Theoretical Study of Heterojunction and Graded Band Gap Type Solar Cells

Annual Report on
NASA Grant No.
NSG 1116

March 1976

J. R. Hauser and J. E. Sutherland

North Carolina State University
Electrical Engineering Department
Box 5275, Raleigh, NC 27607

Table of Contents

# 1. Introduction

This report summarizes research work so far performed on the theory of heterojunction and graded bandgap solar cells. The major objective of the work is to investigate the material compositions and device dimensions needed for high efficiency solar cells. Because of the involved analysis of the fundamental equations describing solar cell operation, a general numerical device analysis program is being used to study solar cells.

A major part of the initial work has been involved in modifying an existing silicon solar cell analysis program to account for the unique features of graded bandgap and heterojunction solar cells. This phase of the work has been completed and the program is now being used to study solar cell performance.

The most successful III-V solar cells have so far been constructed in the GaAs and $Ga_{1-x}Al_xAs$ material systems. Consequently the work reported herein is concerned with such solar cells. The most efficient solar cell so far evaluated is an abrupt heterojunction cell with a pure AlAs layer at the surface with a GaAs substrate. The predicted efficiency for this cell is slightly larger than that of a graded bandgap $Ga_{1-x}Al_xAs$ solar cell.

# 2. Theoretical Concepts of Variable Composition Solar Cells

## 2.1 Features of an Ideal Solar Cell

In order to effectively convert light energy to electrical energy, a solar cell must perform several tasks. First, its surface must transmit, rather than reflect most of the light striking it. Second, the crystal lattice of the cell should absorb the solar photons, exciting electrons out of the valence band and creating electron-hole pairs. Third, built-in fields must separate these excess carriers before they can recombine. Finally, the cell should deliver the carriers to an external load without a large internal resistive loss.

The efficient performance of these tasks calls for several basic device characteristics, not all of which are simultaneously achievable. Outstanding among these ideal characteristics are:

1. Close optical match between cell surface and external medium
2. Efficient absorption of photons in the solar spectrum
3. Carrier generation concentrated in regions of large built-in field and low recombination rate
4. Large open circuit voltage
5. Small bias current under dark conditions
6. Low sheet resistance

## 2.2 Material Parameters Determining Device Characteristics

In order to optimize the solar cell structure, the material parameters that control the device characteristics must be determined. The first characteristic, a reasonably good optical match at the semiconductor surface, can usually be obtained with an appropriate anti-reflection layer that transmits the bulk of the energy at the wavelengths dominating the solar spectrum.

The second characteristic, efficient absorption of photons, is controlled primarily by the value of the band gap and absorption coefficient. Only those photon energies larger than the band gap will create significant numbers of electron-hole pairs. However, when the photon energy greatly exceeds the band gap, much of the excess will be wasted.

The third characteristic calls for carrier generation predominantly near the p-n junction of a cell. Also, carrier generation should not be wasted in regions of high recombination rate, particularly near the surface, where imperfections cannot be entirely eliminated. Since the maximum light intensity always occurs at the cell surface, surface recombination is one of the most difficult problems to solve, especially in III-V solar cells.

Large open circuit voltage calls for a wide band gap semiconductor. However, the wider the band gap, the smaller the fraction of photons having sufficient energy to create electron-hole pairs. Similarly, a small forward dark current depends on a large band gap with the accompanying large built-in potential across the p-n junction.

Finally, a low sheet resistance can be obtained by using a thick surface layer above the p-n junction. However, the thicker the surface layer, the greater the attenuation of light reaching the junction depletion region, the most desirable area of optical generation.

## 2.3 Limitations of Conventional Cells

The fact that conventional solar cells are usually constructed of a single material (usually silicon) severely limits the degree to which the cell characteristics can be influenced. One of the most crucial material parameters, the band gap, becomes fixed as soon as the cell

material is selected. A constant band gap results in a monotonically decreasing optical generation rate. In other words, a homogeneous solar cell concentrates carrier generation near the surface, where the recombination rate is highest, and the built-in field from the p-n junction is relatively weak. If the p-n junction is moved very near the surface to separate the electron-hole pairs more efficiently, the surface layer sheet resistance becomes unacceptably high.

In addition, silicon has a band gap (about 1.1 eV) which is too small to efficiently use the photon energies that dominate the solar spectrum [1,2]. Theoretical calculations have estimated that a band gap value of about 1.4 eV should lead to the most efficient carrier generation by sunlight. Too few solar photons have sufficient energy to bridge larger gaps.

In addition to more efficient carrier generation, a larger band gap semiconductor leads to a higher open circuit voltage [2,19], and lower dark current, both mentioned earlier as desirable characteristics. In short, conventional homogeneous silicon solar cells leave much to be desired in theoretical efficiency. Their main attractiveness stems from the advanced state of silicon technology.

## 2.4 Advantages of Variable Composition Materials

Clearly, the variation of material composition with depth available in III-V semiconductors should permit improved control over the distribution of carrier generation. The band diagram in Fig. 2.1 shows a wide band gap ($E_{g1}$) surface layer covering a smaller band gap ($E_{g2}$) substrate. If $E_{g1}$ is chosen large enough, the surface layer can serve as a window,

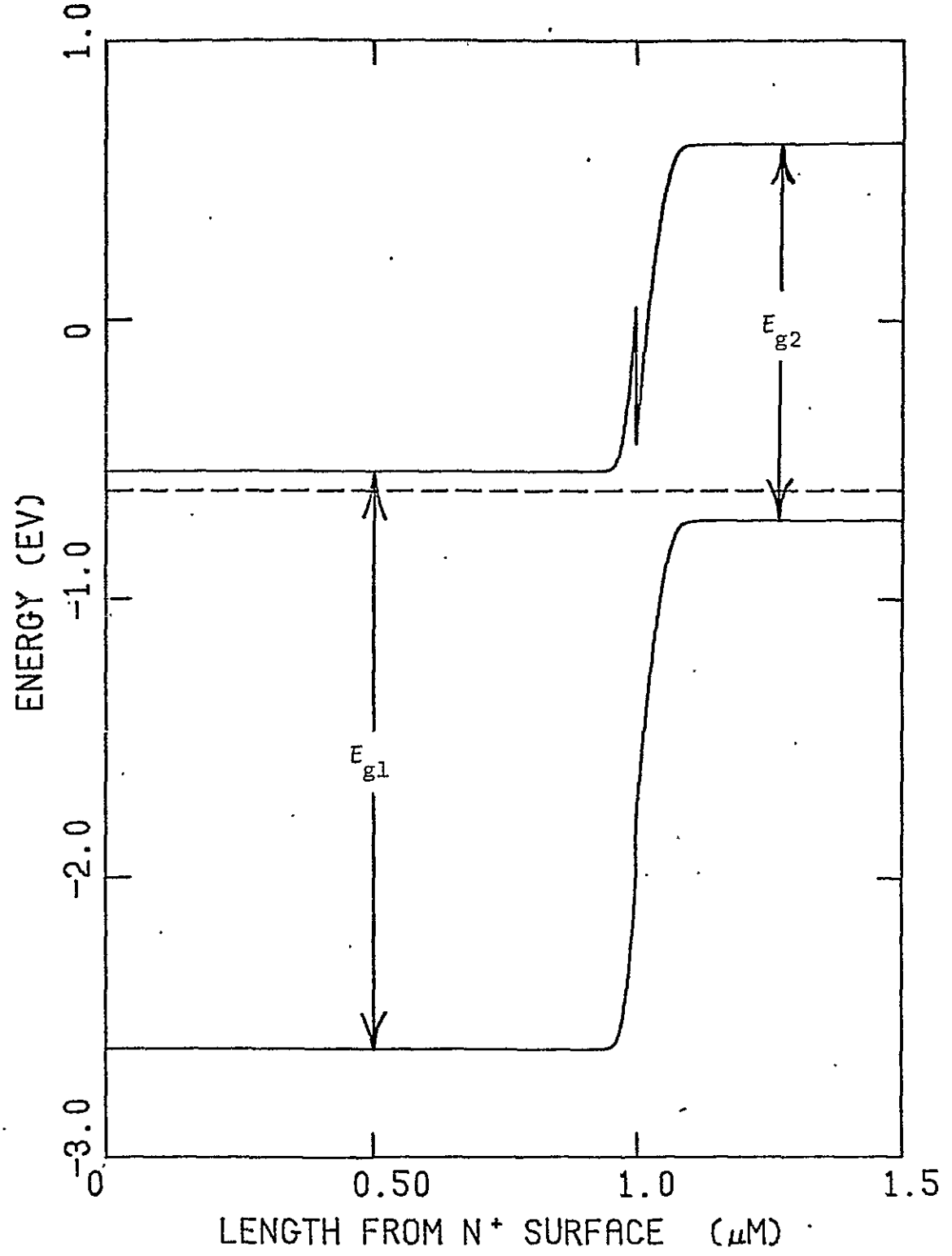


Figure 2.1 Energy band diagram for an n on p heterojunction solar cell

transmitting most photons to the p-n junction where the band gap is smaller. Thus carrier generation can be concentrated in a region of large built-in field, far from surface recombination states. If the concentration of interface states in the regions of variable composition can be kept at acceptable levels, then minority carrier collection should be accomplished with much greater efficiency than in homogeneous solar cells.

In addition, a thick surface layer can be used to reduce sheet resistance without severely attenuating the light intensity reaching the p-n junction. Also, band gap grading can be used to create additional built-in fields that aid carrier collection.[3,4]. In fixed band gap devices, built-in fields must be created by doping gradients. However, if the band gap can also vary, independent effective built-in fields can be made to operate on electrons and on holes:

$$E_{no} = -\frac{1}{q}\frac{d(E_F-E_c)}{dx}$$

$$E_{po} = -\frac{1}{q}\frac{d(E_F-E_v)}{dx}$$

Finally, the cell shown in Fig. 2.1 should have a larger open circuit voltage than a comparable homogeneous cell made of a material with the smaller band gap, $E_{g2}$. At the same time, such a variable gap cell makes effective use of the lower energy photons that would be lost to a homogeneous cell made of a material with the larger band gap, $E_{g1}$.

Thus, the variable composition solar cell appears to be a step closer to the ideal cell described in Sec. 2.1. However, the complexity of the trade-offs involved defies simple approximations. For this reason, a computer analysis program is desirable to give a better estimate of the performance improvement that can be expected.

# 3. Device Equations for Computer Analysis

## 3.1 Equations for Homogeneous Solar Cells

In order to adequately analyze variable band gap solar cells, several device phenomena must be incorporated into the mathematical equations used to model the cells. Many effects included in the present work are important in ordinary homojunction solar cells. Among these are:

1. Drift and diffusion currents
2. Position dependent doping
3. Doping dependent mobility
4. Optical carrier generation
5. Bulk generation-recombination effects
6. Surface recombination effects

The introduction of spatially varying composition demands that additional factors be accounted for:

1. Position dependent band gap
2. Position dependent electron affinity
3. Built in fields due to a varying band gap
4. Composition dependent refractive index at the surface
5. Other position dependent material parameters such as:
   a. mobility
   b. dielectric constant
   c. optical absorption coefficient

The basic semiconductor equations used for homojunction devices can be modified to model variable composition device behavior. The unmodified equations in one dimension are [5-9]:

Transport:

$$J_n = q\mu_n nE + q D_n \frac{\partial n}{\partial x}, \tag{3.1}$$

$$J_p = q\mu_p pE - q D_p \frac{\partial p}{\partial x}, \tag{3.2}$$

Continuity:

$$\frac{\partial n}{\partial t} = -U + \frac{1}{q}\frac{\partial J_n}{\partial x} + G_e, \tag{3.3}$$

$$\frac{\partial p}{\partial t} = -U - \frac{1}{q}\frac{\partial J_p}{\partial x} + G_e, \tag{3.4}$$

Poisson's equation:

$$\frac{\partial E}{\partial x} = \frac{q}{\varepsilon}(p-n+N), \tag{3.5}$$

Auxilliary equations:

$$U = \frac{np-n_i^2}{\tau_{no}(p+p_1)+\tau_{po}(n+n_1)}, \tag{3.6}$$

(Shockley-Read-Hall model with single trapping level)

$$n = N_c \exp\left[\frac{E_{Fn}-E_c}{kT}\right] \text{ (non-degenerate)}, \tag{3.7}$$

$$p = N_v \exp\left[\frac{E_v-E_{Fp}}{kT}\right] \text{ (non-degenerate)}, \tag{3.8}$$

$$N = N_D^+ - N_A^- \text{ (net doping)} \tag{3.9}$$

(N>0 for n-type).

This system of equations is valid only for a device made of a single semiconductor material doped with enough impurities to create the desired doping profile. The electron energy band structure and its associated characteristics must be the same throughout the device.

The existing computer device analysis program for homogeneous solar cells [9] depends on the fact that the preceding group of equations can be reduced to three equations in the three unknowns: $\psi$, $\phi_n$, and $\phi_p$, where $\psi$ is the electrostatic potential and $\phi_n$ and $\phi_p$ are the Fermi potentials defined by:

$$\phi_n = -\frac{1}{q} E_{Fn}, \tag{3.10}$$

$$\phi_p = -\frac{1}{q} E_{Fp}. \tag{3.11}$$

It can be shown that the same basic approach using the same three variables, can be used to analyze variable composition solar cells. The modifications required to account for material variations are discussed in the next section.

## 3.2 Modification of Equations to Allow for Variable Composition

In order to rewrite the device equations so that they apply to variable composition devices, it is useful to recall the basic principles from which they were derived. In particular, Equations (3.1) and (3.2) can be written as:

$$J_n = \mu_n n \frac{d E_{Fn}}{dx} \tag{3.12}$$

$$J_p = \mu_p p \frac{d E_{Fp}}{dx} \tag{3.13}$$

For a homogeneous material, it can be seen that Equations (3.1) and (3.2) result from Equations (3.12) and (3.13) in the following manner. From Figure 3.1:

$$E_c = q\psi_o - q\psi - \chi_c, \tag{3.14}$$

and

$$E_v = q\psi_o - q\psi - \chi_c - E_g. \tag{3.15}$$

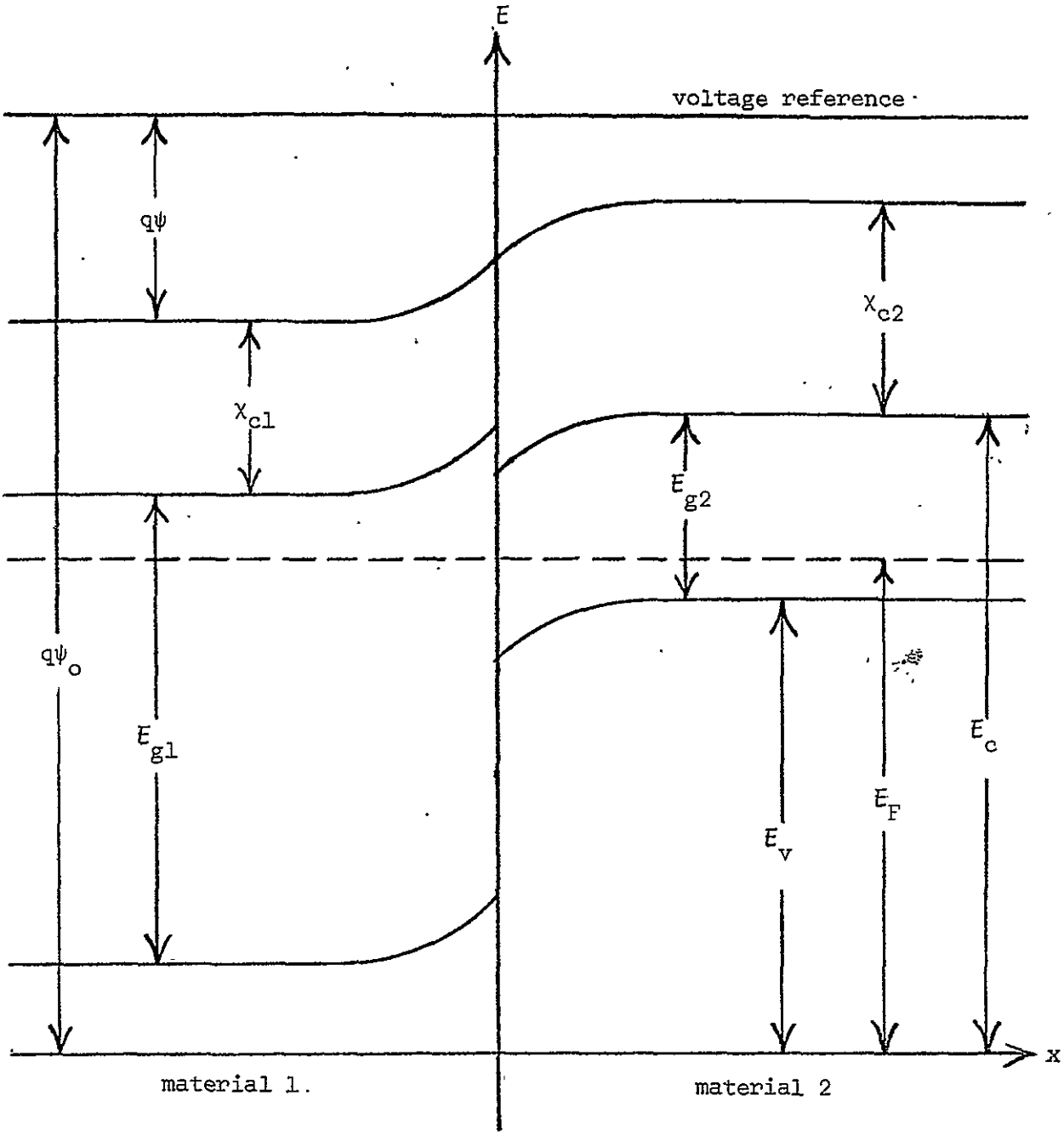


Figure 3.1 Equilibrium energy band diagram for a heterojunction solar cell

From equations (3.7) and (3.8),

$$E_{Fn} = E_c + kT \ln \left(\frac{n}{N_c}\right), \tag{3.16}$$

$$E_{Fp} = E_v - kT \ln \left(\frac{p}{N_v}\right). \tag{3.17}$$

Using Equations (3.14) and (3.16), Equation (3.12) can be rewritten as:

$$J_n = \mu_n n \frac{d}{dx}\left[q\psi_o - q\psi - \chi_c + kT \ln\left(\frac{n}{N_c}\right)\right], \tag{3.18}$$

$$= \mu_n n \left[qE - \frac{d\chi_c}{dx} + \frac{kT}{n}\frac{dn}{dx} - \frac{kT}{N_c}\frac{dN_c}{dx}\right].$$

And, using Equations (3.15) and (3.17), Equation (3.13) can be rewritten as:

$$J_p = \mu_p p \frac{d}{dx}\left[q\psi_o - q\psi - \chi_c - E_g - kT \ln\left(\frac{p}{N_v}\right)\right], \tag{3.19}$$

$$= \mu_p p \left[qE - \frac{d\chi_c}{dx} - \frac{dE_g}{dx} - \frac{kT}{p}\frac{dp}{dx} + \frac{kT}{N_v}\frac{dN_v}{dx}\right].$$

For a homogeneous material, $\chi_c$, $E_g$, $N_c$, and $N_v$ are constant throughout the device. Therefore, Equations (3.18) and (3.19) simplify to Equations (3.1) and (3.2). But for a variable composition structure, Equations (3.1) and (3.2) must be replaced by Equations (3.18) and (3.19), or by the simpler forms of Equations (3.12) and (3.13).

The continuity Equations, (3.3) and (3.4), apply equally well to heterogeneous or homogeneous materials. Poisson's equation, however, fails to reduce to the simple expression of equation (3.5) when composition (and therefore dielectric constant, $\varepsilon$) is allowed to vary with position. A more general form can be derived as follows.

Basically Poisson's equation in one dimension is

$$\frac{dD}{dx} = \rho$$

$$\frac{d(\varepsilon E)}{dx} = q(p-n+N)$$

$$\varepsilon \frac{dE}{dx} + E \frac{d\varepsilon}{dx} = q\,(p-n+N)$$

$$\frac{d^2\psi}{dx^2} = -\frac{q}{\varepsilon}(p-n+N) - \frac{d\psi}{dx}\,\frac{d\varepsilon}{dx} \tag{3.20}$$

Thus, when the dielectric constant becomes a function of position, Equation (3.20) must replace Equation (3.5).

The carrier concentration equations demand no modification, but they can be written in a more convenient form for the purposes of computer analysis. Using Equations (3.10), (3.11), (3.14) and (3.15), Equations (3.7) and (3.8) become:

$$n = n_{i2} \exp\left[\frac{q}{kT}\left(\psi-\phi_n+\frac{\chi_c}{q} - \psi_o + \frac{kT}{q}\ln\frac{N_c}{n_{i2}}\right)\right]$$

$$p = n_{i2} \exp\left[\frac{q}{kT}\left(\phi_p-\psi-\frac{\chi_c}{q} - \frac{E_g}{q} + \psi_o + \frac{kT}{q}\ln\frac{N_v}{n_{i2}}\right)\right]$$

where $n_{i2}$ = intrinsic carrier concentration of material #2 in the alloy.

The composition dependent (and therefore position dependent) parameters can be grouped into two terms

$$\theta_n = \frac{\chi_c}{q} - \psi_o + \frac{kT}{q}\ln\frac{N_c}{n_{i2}}, \tag{3.21}$$

$$\theta_p = -\frac{1}{q}(\chi_c+E_g) + \psi_o + \frac{kT}{q}\ln\frac{N_v}{n_{i2}} \tag{3.22}$$

Then, the carrier density equations can be written concisely as

$$n = n_{i2} \exp\left\{\frac{q}{kT}\left[\psi-\phi_n + \theta_n\right]\right\}, \tag{3.23}$$

$$p = n_{i2} \exp\left\{\frac{q}{kT}\left[\phi_p-\psi+\theta_p\right]\right\}. \tag{3.24}$$

These expressions are analgous to the forms used in the computer analysis of homogeneous solar cells [9]:

$$n = n_i \exp\left[\frac{q}{kT}(\psi-\phi_n)\right],$$

$$p = n_i \exp\left[\frac{q}{kT}(\phi_p-\psi)\right].$$

The parameters, $\theta_n$ and $\theta_p$ depend only on composition, and must be externally supplied as functions of position after the composition profile is specified. The use of these parameters is discussed further in Sec. 4.3.5.

The other auxilliary equations remain the same whether or not composition is spatially varying. However, it is important to note that several variables no longer can be assumed to be constant. In fact, the material parameters $\mu_n$, $\mu_p$, $\varepsilon$, $n_i$, $n_1$ and $p_1$ must be given as known functions of composition (or position, when the composition profile is known).

Thus, the complete one dimensional mathematical model for variable composition solar cells consists of the following system of equations:

$$J_n = \mu_n n \frac{dE_{Fn}}{dx}, \tag{3.25}$$

$$J_p = \mu_p p \frac{dE_{Fp}}{dx}, \tag{3.26}$$

$$\frac{\partial n}{\partial t} = G_e - U + \frac{1}{q}\frac{dJ_n}{dx}, \tag{3.27}$$

$$\frac{\partial p}{\partial t} = G_e - U - \frac{1}{q}\frac{dJ_p}{dx}, \tag{3.28}$$

$$\frac{d^2\psi}{dx^2} = -\frac{q}{\varepsilon}(p-n+N) - \frac{d\psi}{dx}\frac{d\varepsilon}{dx}, \tag{3.29}$$

$$U = \frac{np - n_i^2}{\tau_{no}(p+p_1) + \tau_{po}(n+n_1)}, \tag{3.30}$$

$$n = n_{i2} \exp\left[\frac{q}{kT}(\psi - \phi_n + \theta_n)\right], \tag{3.31}$$

$$p = n_{i2} \exp\left[\frac{q}{kT}(\phi_p - \psi + \theta_p)\right], \tag{3.32}$$

with auxilliary equations:

$$E_{Fn} = -q\,\phi_n, \tag{3.33}$$

$$E_{Fp} = -q\,\phi_p, \tag{3.34}$$

and with the following parameters given as functions of position:

$N = N(x) = N_D^+ - N_A^-$, net doping profile (3.35)

$C = C(x)$, composition profile (3.36)

(for example, C = mole fraction, x, of AlAs in an $Al_xGa_{1-x}As$ solar cell)

$\mu_n = \mu_n(x)$, electron mobility (3.37)

$\mu_p = \mu_p(x)$, hole mobility (3.38)

$\varepsilon = \varepsilon(x)$, dielectric constant (3.39)

$n_i = n_i(x)$, intrinsic carrier concentration (3.40)

$n_1 = n_1(x)$, trapping center parameter for electrons (3.41)

$p_1 = p_1(x)$, trapping center parameter for holes (3.42)

$\tau_{no} = \tau_{no}(x)$, excess carrier lifetime in $p^+$ material (3.43)

$\tau_{po} = \tau_{po}(x)$, excess carrier lifetime in $n^+$ material (3.44)

$E_g = E_g(x)$, band gap (3.45)

$\theta_n = \theta_n(x)$, conduction band parameter (3.46)

$\theta_p = \theta_p(x)$, valence band parameter (3.47)

$G_e = G_e(x)$, optical generation rate (3.48)

Magnetic effects and thermal gradients are assumed to be negligible. The modeling of several of the above parameters will be discussed in the following sections.

This apparently unwieldy mathematical system can actually be reduced to three equations in three unknowns in exactly the same manner used for homogeneous solar cells in previous computer models. The fact that composition (and the associated material parameters) is allowed to vary through the cell simply adds some complexity to the detailed computations without altering the method of solution. For this reason, it has been possible to modify an existing computer analysis program designed for silicon homojunction solar cells [9], in order to permit analysis of variable composition cells. A major share of the work up to the present time has been devoted to these detailed modifications. However, the modified program is now essentially complete and has been used to examine several heterojunction and graded band gap structures. The results of these studies will be discussed in a later section. First, however, the modeling of several of the material parameters deserves some explanation.

# 4. Specific Device Parameter Modeling

## 4.1 Introduction

The modeling modifications discussed in the following sections have been used to convert a computer program designed for a single homogeneous material (silicon) into a program capable of examining a spatially varying alloy of two compatible semiconductors. Given the material properties of the two semiconductors, the program can theoretically analyze the performance of a solar cell of any specified composition profile. For example, solar cells made of the alloy, $Al_xGa_{1-x}As$, have been analyzed by providing the material properties of AlAs and GaAs, along with the desired composition profile, i.e. the mole fraction of AlAs, x, vs. position. Because experimental data concerning the properties of semiconductors and their alloys is limited, reasonable approximations must be used to predict the properties of arbitrary alloys. Whenever possible, these approximations have been checked against experimental results and adjusted to improve the agreement with available data. The most important approximations are described in the following sections.

## 4.2 Dielectric Constant vs. Composition

Given the low frequency dielectric constants, $\varepsilon_{\ell 1}$ and $\varepsilon_{\ell 2}$, for semiconductors 1 and 2, the following interpolation scheme is used to estimate the constant, $\varepsilon_\ell$, for an alloy that has mole fraction, C, of material 1, [20]:

$$\varepsilon_\ell = \frac{1}{\varepsilon_{\ell 2}} \left\{ \frac{1+2\left[C\left(\frac{\varepsilon_{\ell 1}-1}{\varepsilon_{\ell 1}+2}\right)+(1-C)\left(\frac{\varepsilon_{\ell 2}-1}{\varepsilon_{\ell 2}+2}\right)\right]}{1-C\left(\frac{\varepsilon_{\ell 1}-1}{\varepsilon_{\ell 1}+2}\right)-(1-C)\left(\frac{\varepsilon_{\ell 2}-1}{\varepsilon_{\ell 2}+2}\right)} \right\} \qquad (4.1)$$

Exactly the same form is used to estimate the high frequency relative dielectric constant, $\varepsilon_h$, for an alloy:

$$\varepsilon_h = \frac{1}{\varepsilon_{h2}} \left\{ \frac{1+2\left[C\left(\frac{\varepsilon_{h1}-1}{\varepsilon_{h1}+2}\right)+(1-C)\left(\frac{\varepsilon_{h2}-1}{\varepsilon_{h2}+2}\right)\right]}{1-C\left(\frac{\varepsilon_{h1}-1}{\varepsilon_{h1}+2}\right)-(1-C)\left(\frac{\varepsilon_{h2}-1}{\varepsilon_{h2}+2}\right)} \right\} \qquad (4.2)$$

## 4.3 Band Structure Parameters vs. Composition

The original homogeneous solar cell program was based on the assumption that the material being studied had a band structure with a single dominant conduction band valley, either direct or indirect. However, it is possible for a variable composition solar cell to be constructed of an alloy of a direct band gap material and an indirect band gap material [10,11]. Depending on the relative conduction band minima of the two materials and the alloy composition, it is possible that two conduction band valleys (one direct and one indirect) significantly affect carrier behavior.

In order to allow for such a situation, the modified program permits the specification of two valleys, each with its own composition dependent band gap and its own characteristic effective mass and mobility. The following sections describe the techniques used to determine the resultant band structure parameters (such as electron and hole mobilities) of an alloy, when the band structure parameters for each of the two components are given.

### 4.3.1 Band Gap vs. Composition

Referring to Figure 4.1, the resultant direct and indirect band gaps are estimated empirically from the gaps of the component materials.

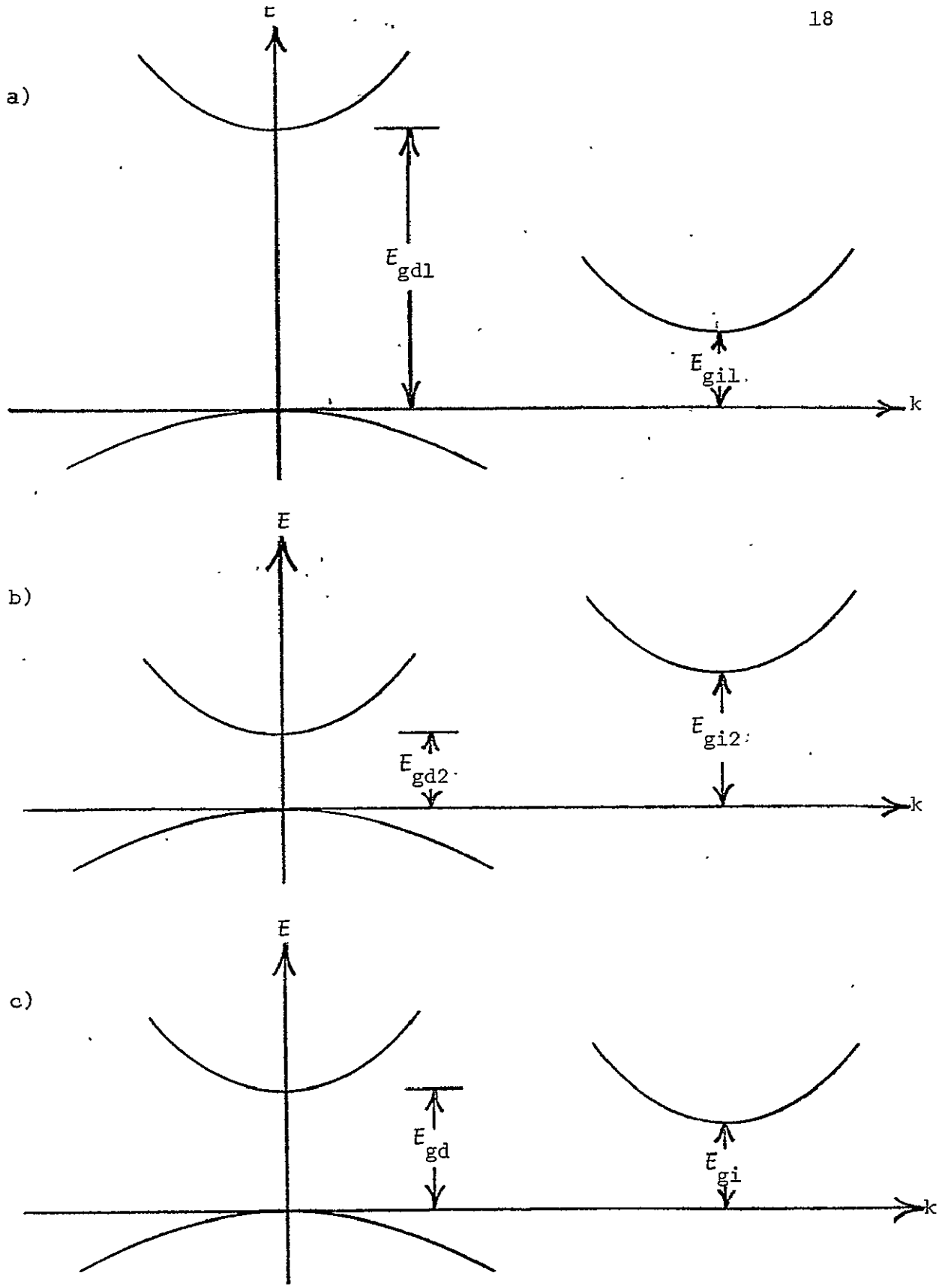


Figure 4.1 Electron energy, E, vs. wave vector, k, for a) indirect semiconductor, material 1, b) direct semiconductor, material 2, c) alloy of materials 1 and 2

Experimental studies have shown that when two materials having direct gaps, $E_{gd1}$ and $E_{gd2}$, are alloyed, the resulting direct gap has a quadratic dependence on composition:

$$E_{gd} = a\,C^2 + bC + E_{gd2} \tag{4.3}$$

where C = mole fraction of material 1, and a and b are adjusted for closest fit to the experimental data. For $Al_xGa_{1-x}As$, the indirect gap was estimated by linear interpolation:

$$E_{gi} = E_{gi1} + (E_{gi2}-E_{gi1})(1-C) \tag{4.4}$$

The resultant alloy band gap is, of course, given by:

$$E_g = \text{Minimum of } (E_{gd}, E_{gi}) \tag{4.5}$$

### 4.3.2 Effective Masses

The next task is to determine the effective masses for holes and electrons. Since the valence band in each of the two semiconductors is assumed to have a single dominant valley with a characteristic effective mass, it is simply necessary to interpolate between the two effective masses to find the resultant hole effective mass for the alloy. The following interpolation form was used [20]:

$$\frac{1}{m_p^*} = \frac{C}{m_{p1}^*} + \frac{1-C}{m_{p2}^*} \tag{4.6}$$

where $m_{p1}^*$ = hole effective mass in material 1

$m_{p2}^*$ = hole effective mass in material 2

$m_p^*$ = hole effective mass in alloy

C = mole fraction of material 1

The same form was used to find the electron effective mass for the direct valley:

$$\frac{1}{m^*_{cd}} = \frac{C}{m^*_{cd1}} + \frac{1-C}{m^*_{cd2}} \tag{4.7}$$

where $m^*_{cd1}$ = conduction band effective mass in direct valley for material 1.

$m^*_{cd2}$ = conduction band effective mass in direct valley for material 2.

$m^*_{cd}$ = conduction band effective mass in direct valley for alloy

and likewise for the indirect valley:

$$\frac{1}{m^*_{ci}} = \frac{C}{m^*_{ci1}} + \frac{1-C}{m^*_{ci2}} \tag{4.8}$$

Now, it will prove useful to define, if possible, a single effective mass for all electrons. This can be done in the following way:

$$n = N_{cd} \exp[\frac{E_{Fn}-E_{cd}}{kT}] + N_{ci} \exp[\frac{E_{Fn}-E_{ci}}{kT}]$$

where $N_{cd}$ = direct valley effective density of states

$N_{ci}$ = indirect valley effective density of states

$E_{cd}$ = direct valley minimum

$E_{ci}$ = indirect valley minimum

It is desired to obtain the following form:

$$n = N_c \exp[\frac{E_{Fn}-E_c}{kT}]$$

where $N_c$ = effective density of states for entire conduction band

$E_c$ = absolute minimum of conduction band (the lesser of $E_{cd}$ and $E_{ci}$)

Since $N_{cd} = K\, m^{*3/2}_{cd}$

$N_{ci} = K\, m^{*3/2}_{ci}$

$N_{c} = K\, m^{*3/2}_{n}$

where K is a proportionality constant and $m^*_n$ = effective mass for all electrons.

Then,

$$m^{*3/2}_{n} \exp\left[\frac{E_{Fn}-E_c}{kT}\right] = m^{*3/2}_{cd} \exp\left[\frac{E_{Fn}-E_{cd}}{kT}\right] + m^{*3/2}_{ci} \exp\left[\frac{E_{Fn}-E_{ci}}{kT}\right]$$

$$m^*_n = \left[m^{*3/2}_{cd} \exp\left(\frac{E_c-E_{cd}}{kT}\right) + m^{*3/2}_{ci} \exp\left(\frac{E_c-E_{ci}}{kT}\right)\right]^{2/3}$$

or, in terms of band gaps:

$$m^*_n = \left[m^{*3/2}_{cd} \exp\left(\frac{E_g-E_{gd}}{kT}\right) + m^{*3/2}_{ci} \exp\left(\frac{E_g-E_{gi}}{kT}\right)\right]^{2/3} \qquad (4.9)$$

where $E_{gd}$, $E_{gi}$, $E_g$, $m^*_{cd}$ and $m^*_{ci}$ are given by Equations (4.3), (4.4), (4.5), (4.7) and (4.8).

### 4.3.3 Hole Mobility

Thus far, the effective masses for holes and electrons have been determined as functions of composition when the material parameters of the two alloy components are given. Since the device equations used to model the solar cell require mobility data, instead of effective mass, the final step is to determine hole and electron mobilities.

Mobility depends not only upon host material composition, but upon the doping level as well. In order to calculate hole mobility for

arbitrary doping and composition, an empirical formula, $f_{p2}$, was constructed to approximate the doping dependence of hole mobility for one of the alloy components, to be referred to as material 2:

$$\mu_{p2} = f_{p2}(N) \tag{4.10}$$

where N = total impurity concentration

Now, because

$$\mu_p = \frac{q\langle\tau_p\rangle}{m_p^*} = \mu_{p2}\,\frac{m_{p2}^*}{\langle\tau_{p2}\rangle}\,\frac{\langle\tau_p\rangle}{m_p^*} \tag{4.11}$$

it is apparent that if $\langle\tau_p\rangle$ and $m_p^*$ can be specified as functions of composition, then a reasonable approximation to hole mobility for any doping level and composition can be made. If mobility is controlled primarily by polar optical phonon scattering, then $\langle\tau_p\rangle$ can be written as [21]:

$$\langle\tau_p\rangle = \frac{K}{\sqrt{m_p^*}\,\left(\frac{1}{\varepsilon_h} - \frac{1}{\varepsilon_\ell}\right)} \tag{4.12}$$

where K is a proportionality constant for all materials

$\varepsilon_h$ = high frequency relative dielectric constant

$\varepsilon_\ell$ = low frequency relative dielectric constant

Since Equations (4.1), (4.2) and (4.6) give $\varepsilon_\ell$, $\varepsilon_h$, and $m_p^*$ as composition varies, the modeling of hole mobility is virtually complete. Combining Equations (4.10), (4.11) and (4.12):

$$\mu_p(N,C) = \frac{f_{p2}(N)\; m_{p2}^{*\,3/2}\left(\frac{1}{\varepsilon_{h2}} - \frac{1}{\varepsilon_{\ell 2}}\right)}{m_p^{*\,3/2}\left(\frac{1}{\varepsilon_h} - \frac{1}{\varepsilon_\ell}\right)} \tag{4.13}$$

where $m_{p2}^*$, $\varepsilon_{\ell 2}$, and $\varepsilon_{h2}$ are known parameters of material 2,

$f_{p2}(N)$ is an empirical function relating hole mobility and doping in material 2,

and $\varepsilon_\ell$, $\varepsilon_h$, and $m_p^*$ are given as functions of composition by Equations (4.1), (4.2) and (4.6).

This completes the specification of hole mobility as a function of doping, N, and composition, C.

### 4.3.4 Electron Mobility

The modelling of electron mobility is more complex than hole mobility if an alloy of an indirect gap semiconductor (material 1) and a direct gap semiconductor (material 2) is considered. The following method depends on the assumption that the doping dependence of mobility for the for the indirect valley of the alloy can be inferred from data on material 1, and the dependence for the direct band of the alloy can be inferred from data on material 2. Treating the direct and indirect valleys independently, and using exactly the same technique as described for hole mobility, a direct valley electron mobility, $\mu_d$, and an indirect valley electron mobility, $\mu_i$, can be determined as:

$$\mu_d(N,C) = \frac{f_{n2}(N)\, m_{cd2}^{*\,3/2}\left(\frac{1}{\varepsilon_{h2}} - \frac{1}{\varepsilon_{\ell 2}}\right)}{m_{cd}^{*\,3/2}\left(\frac{1}{\varepsilon_h} - \frac{1}{\varepsilon_\ell}\right)} \tag{4.14}$$

$$\mu_i(N,C) = \frac{f_{n1}(N) m_{ci2}^{*\,3/2}\left(\frac{1}{\varepsilon_{h1}} - \frac{1}{\varepsilon_{\ell 1}}\right)}{m_{ci}^{*\,3/2}\left(\frac{1}{\varepsilon_h} - \frac{1}{\varepsilon_\ell}\right)} \tag{4.15}$$

where $m^*_{cd2}$, $m^*_{ci1}$, $\varepsilon_{\ell 2}$, $\varepsilon_{\ell 1}$, $\varepsilon_{h2}$ and $\varepsilon_{h1}$ are known parameters of material 1 and 2,

$f_{n2}(N)$ is an empirical function relating electron mobility to doping for material 2

$f_{n1}(N)$ is an empirical function relating electron mobility to doping for material 1

and $\varepsilon_\ell$, $\varepsilon_h$, $m^*_{cd}$ and $m^*_{ci}$ are given by Equations (4.1), (4.2), (4.7) and (4.8).

Now, the final task is to merge these two mobilities into a single resultant electron mobility. Such an "effective" mobility can be found by weighing the direct and indirect mobilities by their respective electron populations. These can be determined by the following procedure:

define $R_d$ = fraction of free electrons in direct valley

$n_d$ = electron density in direct valley

$n_i$ = electron density in indirect valley

Then,

$$R_d = \frac{n_d}{n_d+n_i} = \frac{N_{cd}\exp(\frac{E_{Fn}-E_{cd}}{kT})}{N_{cd}\exp(\frac{E_{Fn}-E_{cd}}{kT}) + N_{ci}\exp(\frac{E_{Fn}-E_{ci}}{kT})}$$

or,

$$R_d = \frac{1}{1+(\frac{m^*_{ci}}{m^*_{cd}})^{3/2}\exp(\frac{E_{gd}-E_{gi}}{kT})} \qquad (4.16)$$

where the composition dependent parameters are given by Equations (4.3), (4.4), (4.7) and (4.8). Finally, the resultant electron mobility is

$$\mu_n(N,C) = \mu_d R_d + \mu_i(1-R_d) \tag{4.17}$$

where Equations (4.14), (4.15) and (4.16) give $\mu_d$, $\mu_i$, and $R_d$ in terms of composition.

### 4.3.5 Band Parameters, $\theta_n$ and $\theta_p$

In order to model the composition dependence of the band parameters, $\theta_n$ and $\theta_p$, some knowledge of the variation of electron affinity, $\chi_c$, and band gap, $E_g$, must be available. It has been found to be advantageous to select the potential reference, $\psi_o$, so that $\theta_n = \theta_p = 0$ when the mole fraction of material 1 is zero. In other words, $\theta_n$ and $\theta_p$ are zero in regions of the solar cell consisting entirely of material 2. Then, from Equations (3.21) and (3.22):

$$\psi_o = \frac{\chi_{c2}}{q} + \frac{kT}{q} \ell n \left(\frac{N_{c2}}{n_{i2}}\right) \tag{4.18}$$

$$\psi_o = \frac{\chi_{c2} + E_{g2}}{q} - \frac{kT}{q} \ell n \left(\frac{N_{v2}}{n_{i2}}\right) \tag{4.19}$$

The fact that these two conditions are equivalent can be seen by manipulating the well known expression for intrinsic carrier concentration:

$$n_{i2}^2 = n_2 p_2 = N_{c2} \exp\left(\frac{E_F - E_c}{kT}\right) N_{v2} \exp\left(\frac{E_v - E_F}{kT}\right)$$

$$n_{i2}^2 = N_{c2} N_{v2} \exp\left(\frac{-E_{g2}}{kT}\right)$$

$$E_{g2} = -kT \ell n \left(\frac{n_{i2}^2}{N_{c2} N_{v2}}\right) \tag{4.20}$$

Now, inserting Equation (4.18) into (3.21), and (4.19) into (3.22) gives:

$$\theta_n = \frac{\chi_c - \chi_{c2}}{q} + \frac{kT}{q} \ell n \left(\frac{N_c}{N_{c2}}\right) \tag{4.21}$$

$$\theta_p = \frac{\chi_{c2} - \chi_c}{q} + \frac{E_{g2} - E_g}{q} + \frac{kT}{q} \ell n \left(\frac{N_v}{N_{v2}}\right) \tag{4.22}$$

Finally, in terms of effective mass:

$$\theta_n = \frac{\Delta\chi_c}{q} + \frac{3}{2} \frac{kT}{q} \ell n \left(\frac{m_n^*}{m_{n2}^*}\right) \tag{4.23}$$

$$\theta_p = \frac{-(\Delta\chi_c + \Delta E_g)}{q} + \frac{3}{2} \frac{kT}{q} \ell n \left(\frac{m_p^*}{m_{p2}^*}\right) \tag{4.24}$$

where $\Delta\chi_c = \chi_c - \chi_{c2}$

$$\Delta E_g = E_g - E_{g2}$$

Equations (4.23) and (4.24) are the forms used to compute the band parameters for an arbitrary alloy of two materials. The band gap and the effective masses are given as functions of composition by Equations (4.5), (4.6) and (4.9). The modeling of electron affinity vs. composition depends on the experimental data available for the alloy being examined. A typical case of $A\ell_x Ga_{1-x}As$ is discussed in Sec. 5.2.

# 5. Results of the Computer Analysis of $Al_xGa_{1-x}As$ Solar Cells

## 5.1 Introduction

At the present time, the program modifications are essentially complete and the program has been used to examine several heterojunction and variable band gap solar cells made of $Al_xGa_{1-x}As$. As indicated in previous sections, the program requires considerable input data to define material parameters. The following section lists the material specifications and assumptions upon which the results for $Al_xGa_{1-x}As$ are based.

## 5.2 Material Parameters for AlAs, GaAs, and $Al_xGa_{1-x}As$

Material #1: AlAs

Material #2: GaAs

Dielectric constants [22]:

low frequency: $\varepsilon_{L1} = 10.9$

$\varepsilon_{L2} = 13.2$

high frequency: $\varepsilon_{h1} = 8.5$

$\varepsilon_{h2} = 10.9$

Effective Masses [29]:

holes: $m^*_{p1} = 0.85\ m_o$

$m^*_{p2} = 0.68\ m_o$

electrons:

direct valley: $m^*_{cd1} = 0.128\ m_o$

$m^*_{cd2} = 0.0636\ m_o$

indirect valley: $m^*_{ci1} = 0.37\ m_o$

$m^*_{ci2} = 0.39\ m_o$

Intrinsic carrier concentration for GaAs: $n_{i2} = 1.1 \times 10^7 cm^{-3}$

Temperature = 300°K

Trapping Center: Single trapping center assumed to be at center of band gap regardless of alloy composition:

$$n_1 = p_1 = n_i$$

Mobility vs. doping, N:

Holes, data for GaAs used [12]:

$$\mu_{p2} = f_{p2}(N) = \frac{380\ cm^2/v \cdot s}{[1+(3.17 \times 10^{-17} cm^3)N]^{0.266}}$$

where N = impurity sites/$cm^3$,

Electrons, indirect valley (AlAs data used) [23]:

$$\mu_{n1} = f_{n1}(N) = \frac{165\ cm^2/v \cdot s}{[1+(8.1 \times 10^{-17}\ cm^3)N]^{0.13}}$$

Electrons, direct valley (GaAs data used) [12]:

$$\mu_{n2} = f_{n2}(N) = \frac{7200\ cm^2/v \cdot s}{[1+(5.51 \times 10^{-17} cm^3)N]^{0.233}}$$

Band Gap vs. composition:

AlAs: direct gap = $E_{gd1} = 2.95$ eV [14]

indirect gap = $E_{gi1} = 2.16$ eV [15]

overall gap = $E_{g1} = E_{gi1}$

GaAs: direct gap = $E_{gd2} = 1.439$ eV [17]

indirect gap = $E_{gi2} = 1.87$ [17]

overall gap = $E_{g2} = E_{gd2}$

Alloy direct gap, used empirical formula [17]:

$$E_{gd} = 0.468C^2 + 1.042C + 1.439$$

(where C = mole fraction of AlAs)

Alloy indirect gap, used linear interpolation:

$$E_{gi} = 2.16 + 0.29\,(C-1)$$

Electron affinity vs. composition [24]:

$$\Delta\chi_c = -0.85\,(E_g - E_{g2})$$

(Only $\Delta\chi_c = \chi_c - \chi_{c2}$ was required for the analysis. $\chi_{c2}$ was not assigned a value. See sec. 4.3.5)

Lifetimes [27]: $\tau_{no} = 5.3 \times 10^{-9}$ sec

$\tau_{po} = 8.5 \times 10^{-9}$ sec.

(a first order model to be improved later)

Surface recombination velocity:

$S = 10^5$ cm/sec at front surface

$S = 0$ cm/sec at back surface

Solar power density at solar cell surface: 135.3 mw/cm$^2$, [25].

The optical generation rate, $G_e(x)$ deserves some explanation. $G_e(x)$ was calculated by an independent program similar to the one used for homogeneous solar cell analysis [9]. This modified program accepts an arbitrary composition profile of an alloy of two materials covered by an antireflection layer of SiO, of specified thickness. The program can be run in one of two modes: standard mode, and efficiency mode. By using the efficiency mode, it was found that an antireflection layer thickness of 700 Å provided the closest match to the solar spectrum (AM0 conditions) for any mole fraction of AlAs at the surface. The program has been designed to permit specification of either AM0 or AM1 irradiance conditions. However, at the present time, only AM0 conditions have been examined.

The experimental data on the refractive index of GaAs, shown in Figure 5.1 [12], was used to determine the transmission, absorption and reflection coefficients at the surface. For lack of better experimental data, the refractive index of $Al_xGa_{1-x}As$ was assumed to be the same as that for GaAs. This assumption can be easily improved as soon as better data becomes available. The absorption coefficient for $Al_xGa_{1-x}As$ was calculated by interpolating between data for GaAs [16] and AlAs [13]. The results of this interpolation are shown in Figure 5.2 for six values of the mole fraction of AlAs.

Using the same theoretical techniques as in the homogeneous solar cell analysis [9], $G_e(x)$ was calculated for each composition profile and stored for use in the main solar cell analysis program. Typical results are shown in the next section.

## 5.3 Specific Computer Results

Figure 5.3 illustrates the structure and doping profile common to all the $Al_xGa_{1-x}As$ solar cells examined so far. Although only abrupt junction n-on-p devices have been examined, the analysis program permits specification of a Gaussian doping profile, and a p-on-n configuration, as well.

Since the analysis program was completed, seven significant composition profiles have been examined. These profiles are listed in Figure 5.4 alongside the cell numbers assigned to each one. It should be noted that although the p-n junction of each cell coincides with the termination of composition grading, there is no requirement that this be so. The possible advantages of placing the p-n junction inside or completely outside the region of composition grading will be studied in future runs.

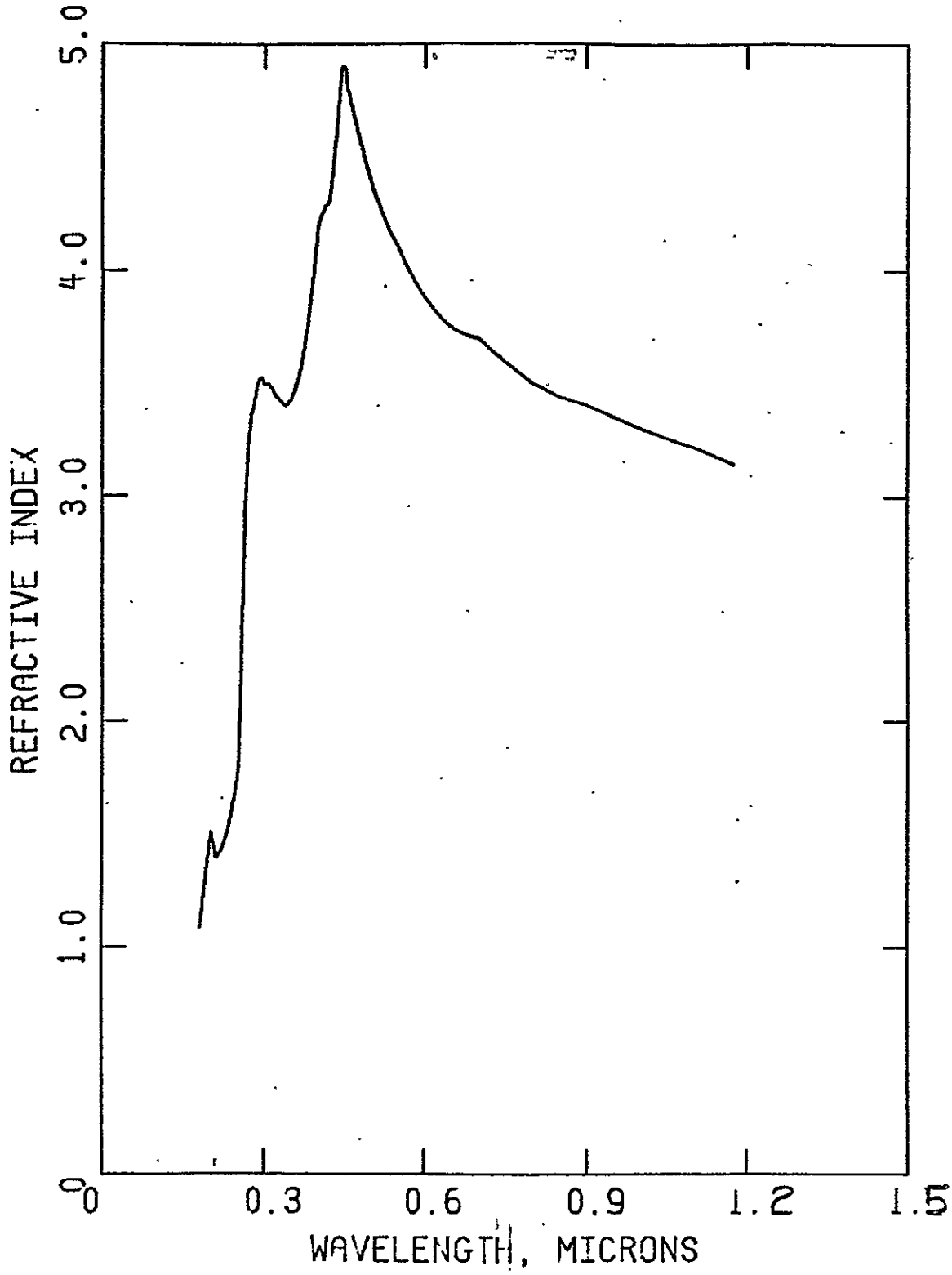


Figure 5.1 Refractive index vs. wavelength for GaAs

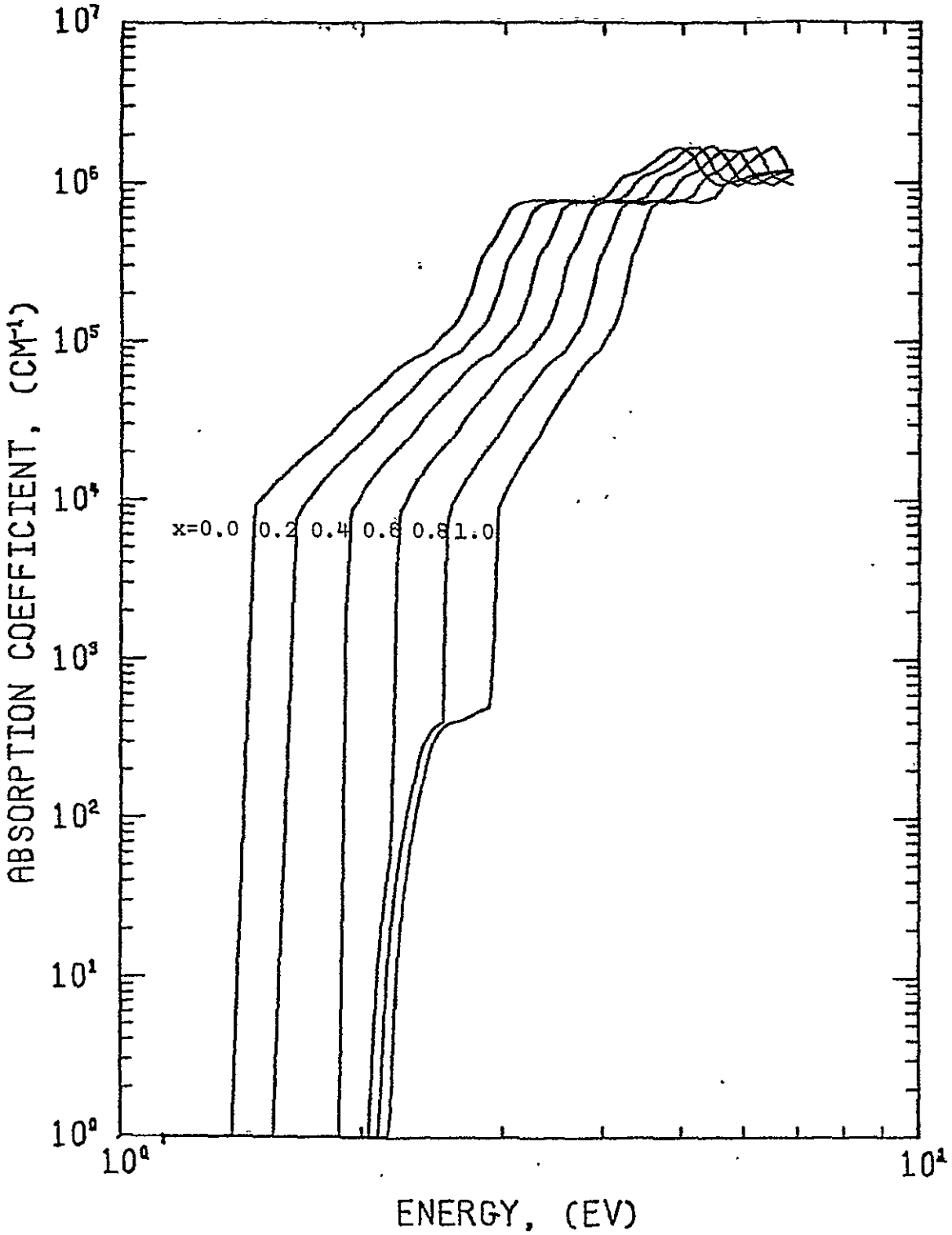


Figure 5.2 Absorption coefficient vs. energy for $Al_xGa_{1-x}As$ with six values of x, mole fraction of AlAs. Interpolated from data on GaAs [16], and AlAs [13]

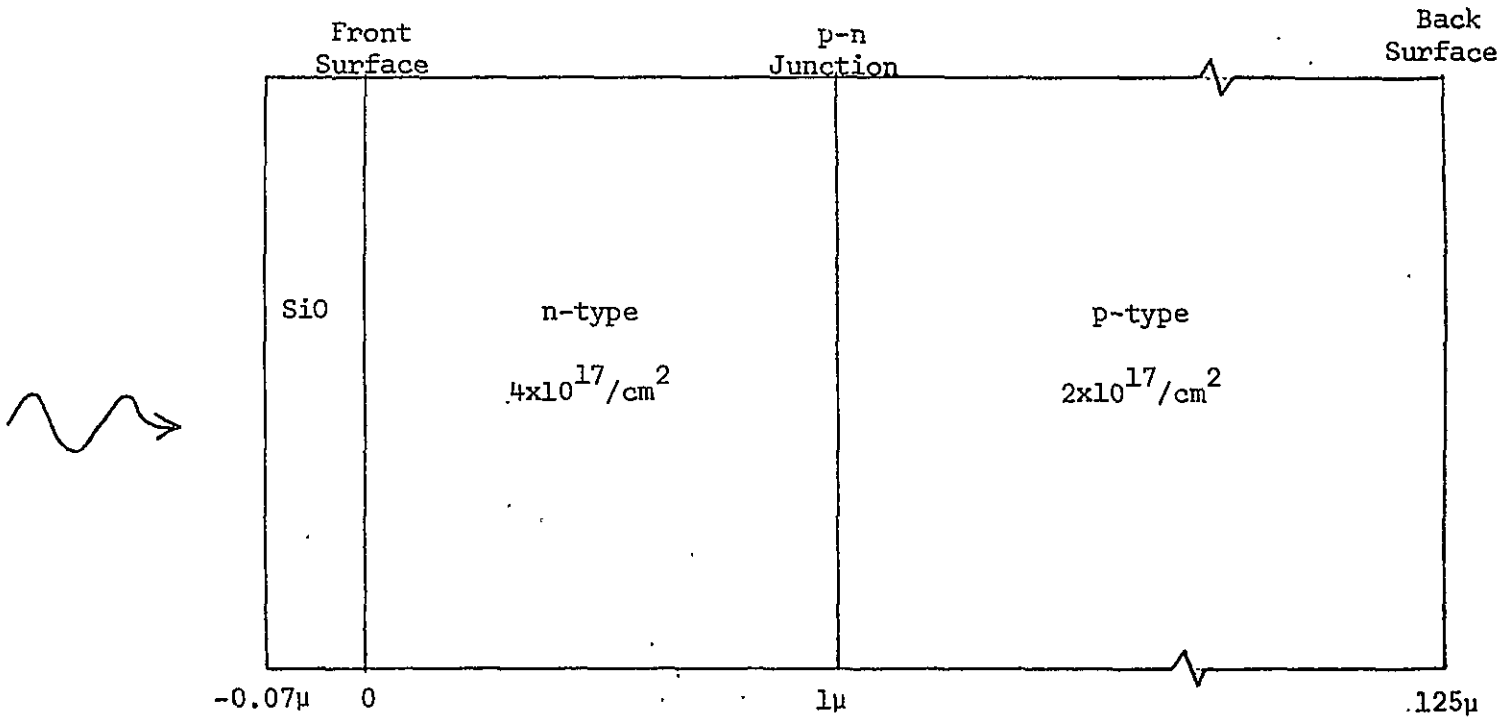


Figure 5.3 Structure and doping levels for all seven cells

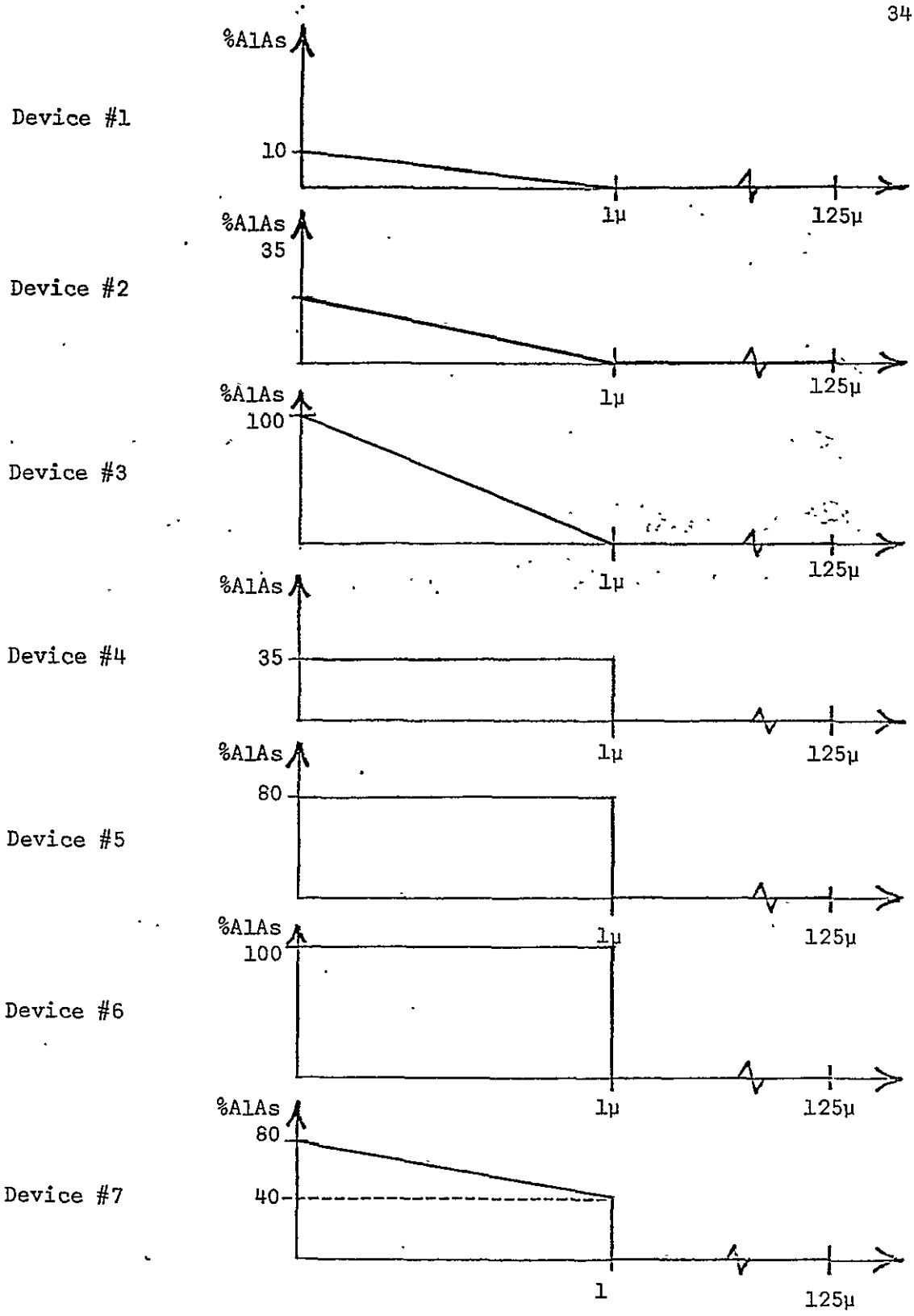


Figure 5.4 Device composition profiles

In order to analyze a solar cell, the computer program requires the specification of device structure along with the desired values of terminal voltage. The results are obtained in both tabular and plotted form. For each value of terminal voltage, the corresponding current density, power density and efficiency are calculated along with the values of electrostatic potential, electron and hole current densities, and electron and hole concentrations at each of approximately 1000 position values. Figures 5.5 through 5.13 present the plotted data for cell 2 as typical of that which has been obtained for each of the devices that has been examined. In the plots covering the entire device (125 μM), the solar cell surface is on the right-hand side, while in the expanded plots, covering only the top layer (1.5 μM), and in the plot of the generation rate, the cell surface is on the lefthand side. It should also be noted that Figures 5.6 through 5.9 plot the absolute magnitude of the current densities, so that sign reversals appear as spikes.

The effects of composition grading are clearly evident in several plots. Figure 5.5 shows the built-in potential resulting from band gap grading as mentioned in Section 2.4. The slope of these curves gives the built-in field. The effect of band gap grading on the optical generation rate can be seen in Figure 5.13, where the reduced slope in the surface layer is due to the absorption of progressively smaller values of photon energy as the band gap shrinks with depth.

The transition from an indirect to a direct band gap structure has a marked effect on device characteristics. Since, for $Al_xGa_{1-x}As$, this transition occurs at about 0.4 mole fraction of AlAs [18], cell 2 consists entirely of a direct gap material, and no transition occurs.

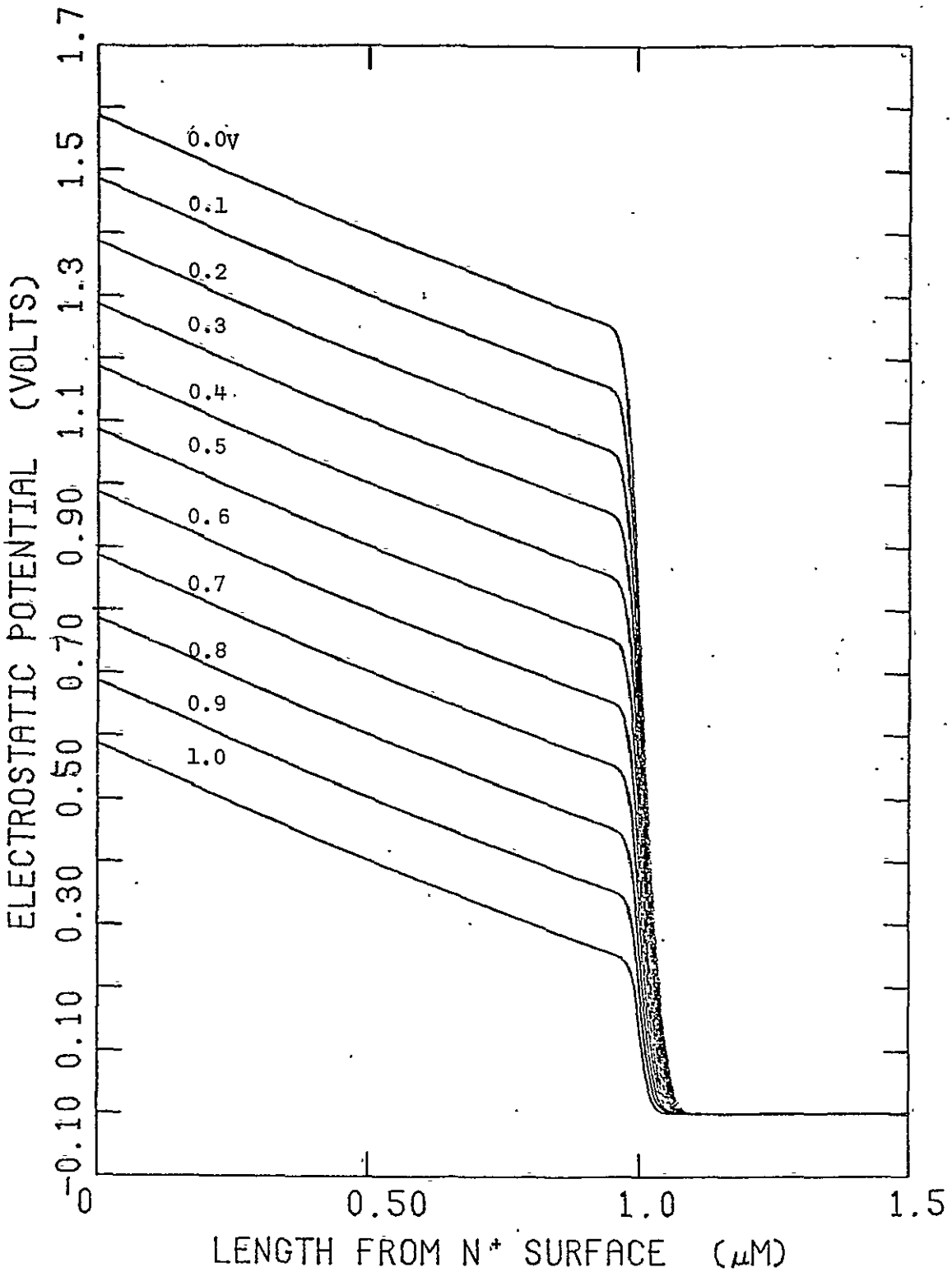


Figure 5.5 Electrostatic potential near the surface for cell 2

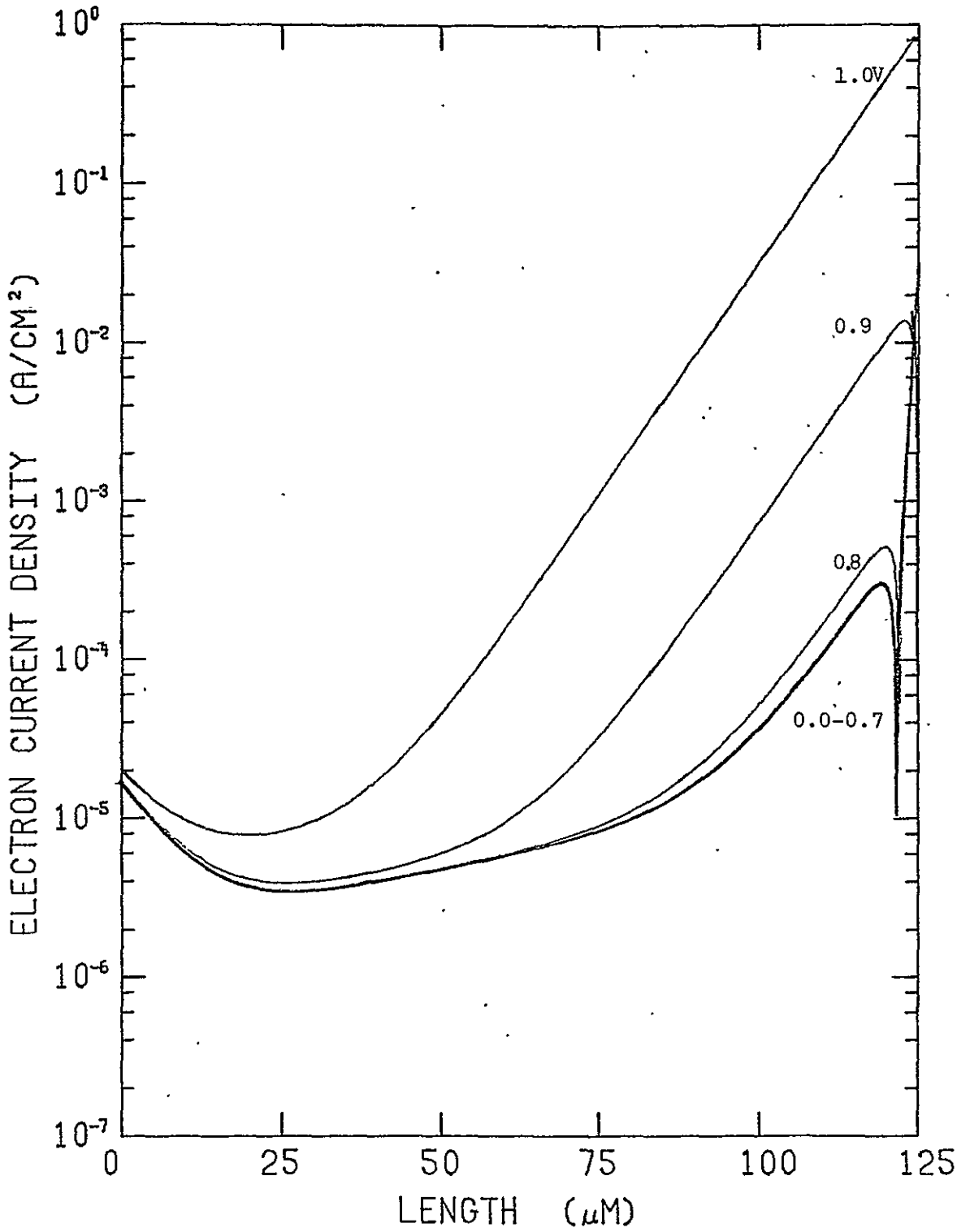


Figure 5.6 Electron current density in cell 2

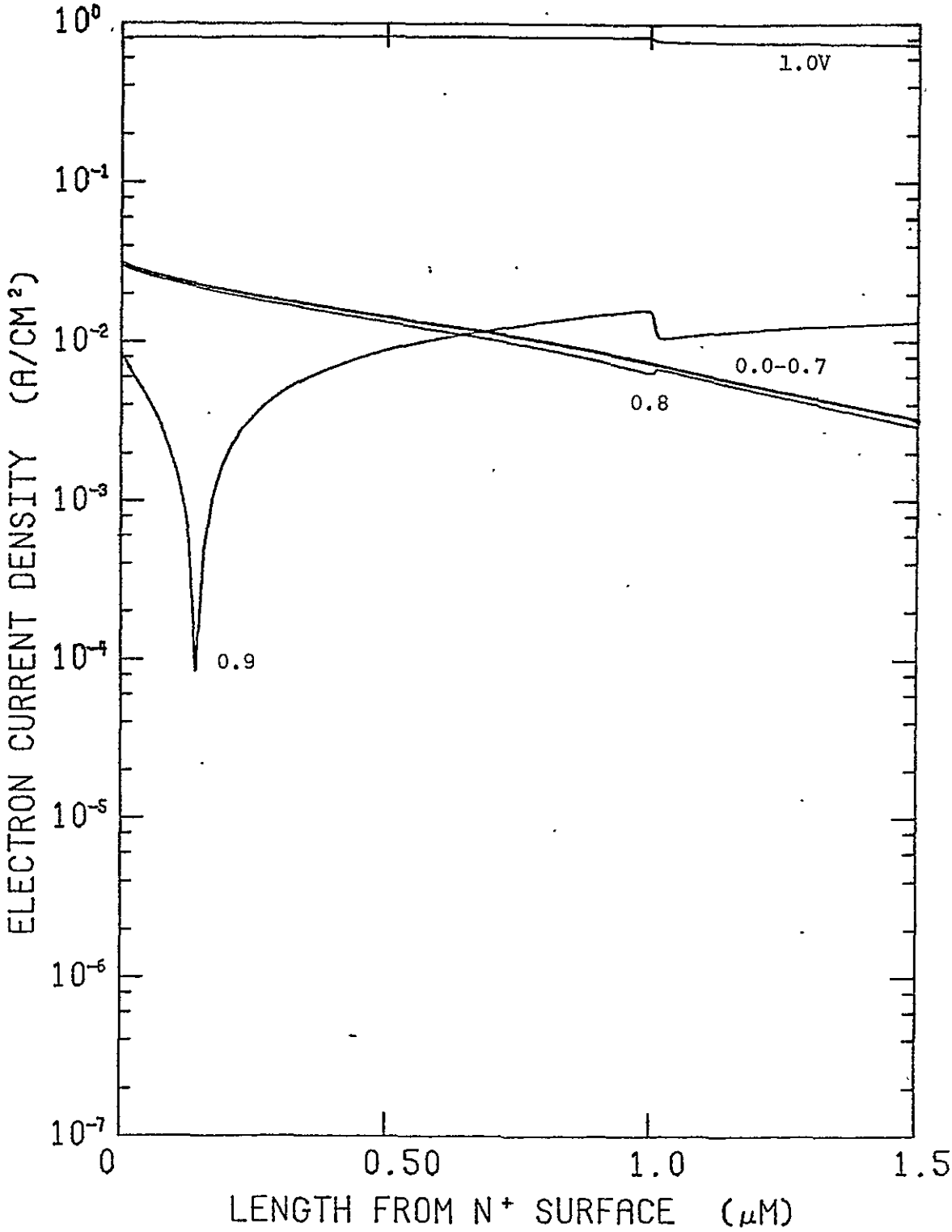


Figure 5.7 Electron current density near the surface of cell 2

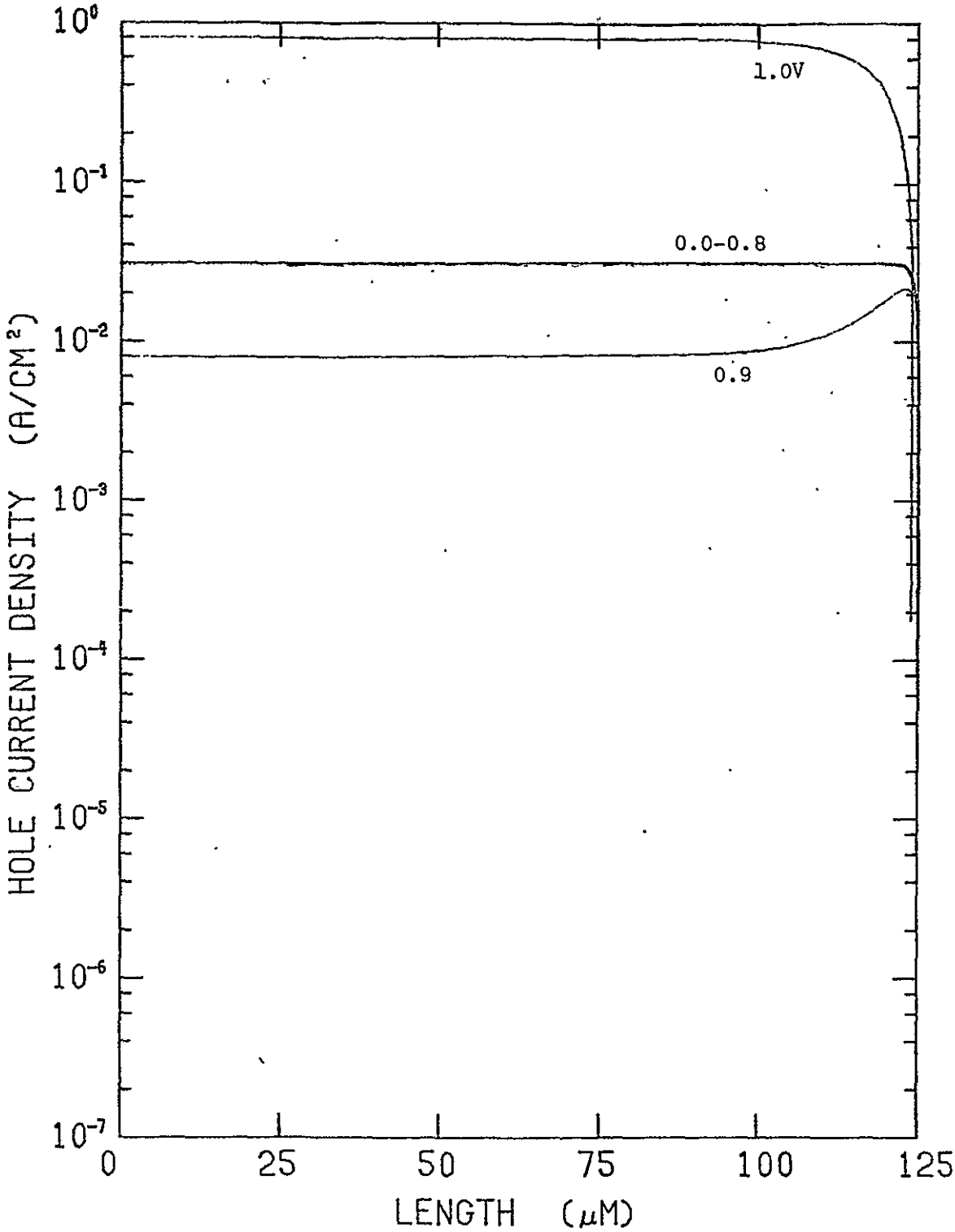


Figure 5.8 Hole current density in cell 2

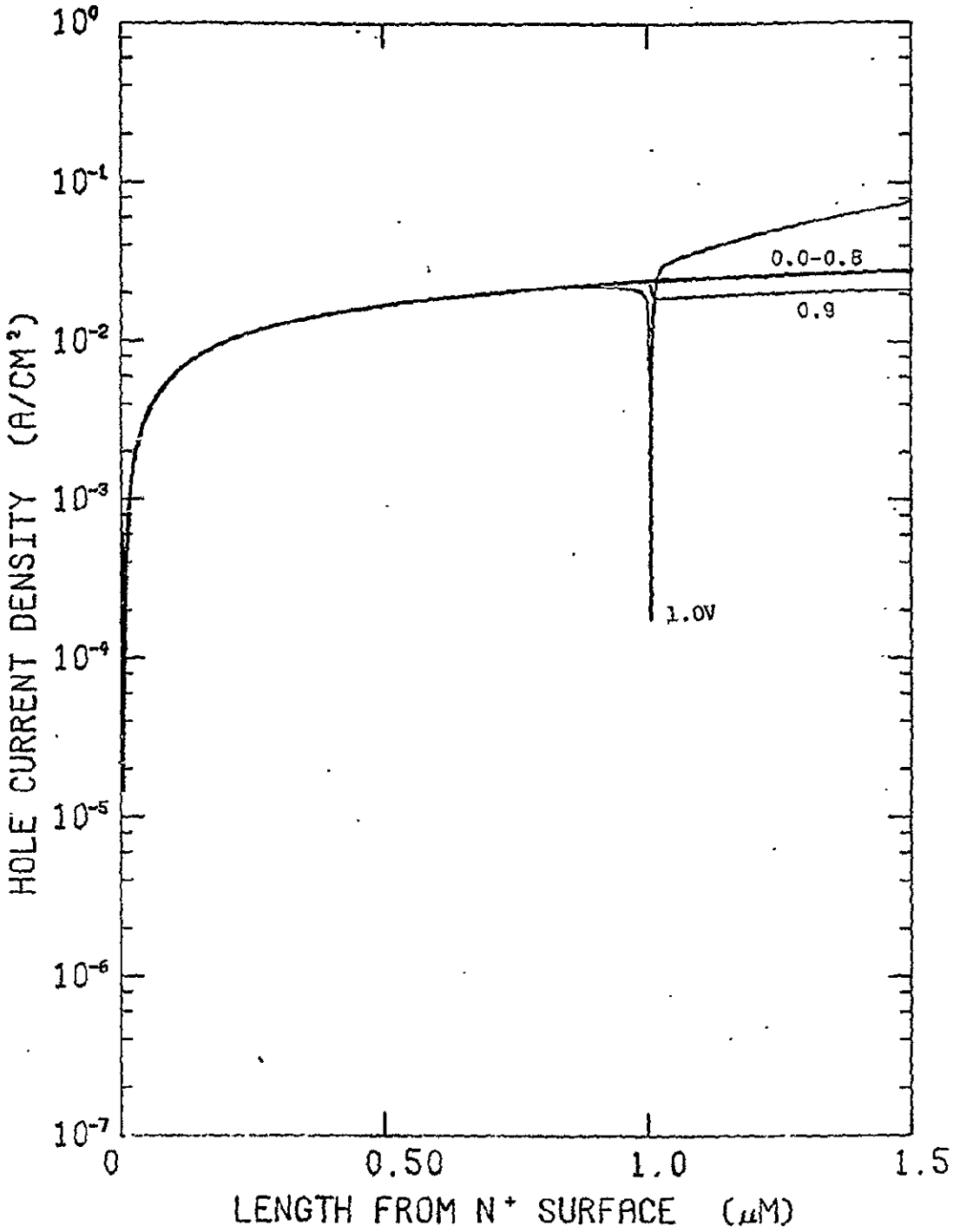


Figure 5.9 Hole current density near the surface of cell 2

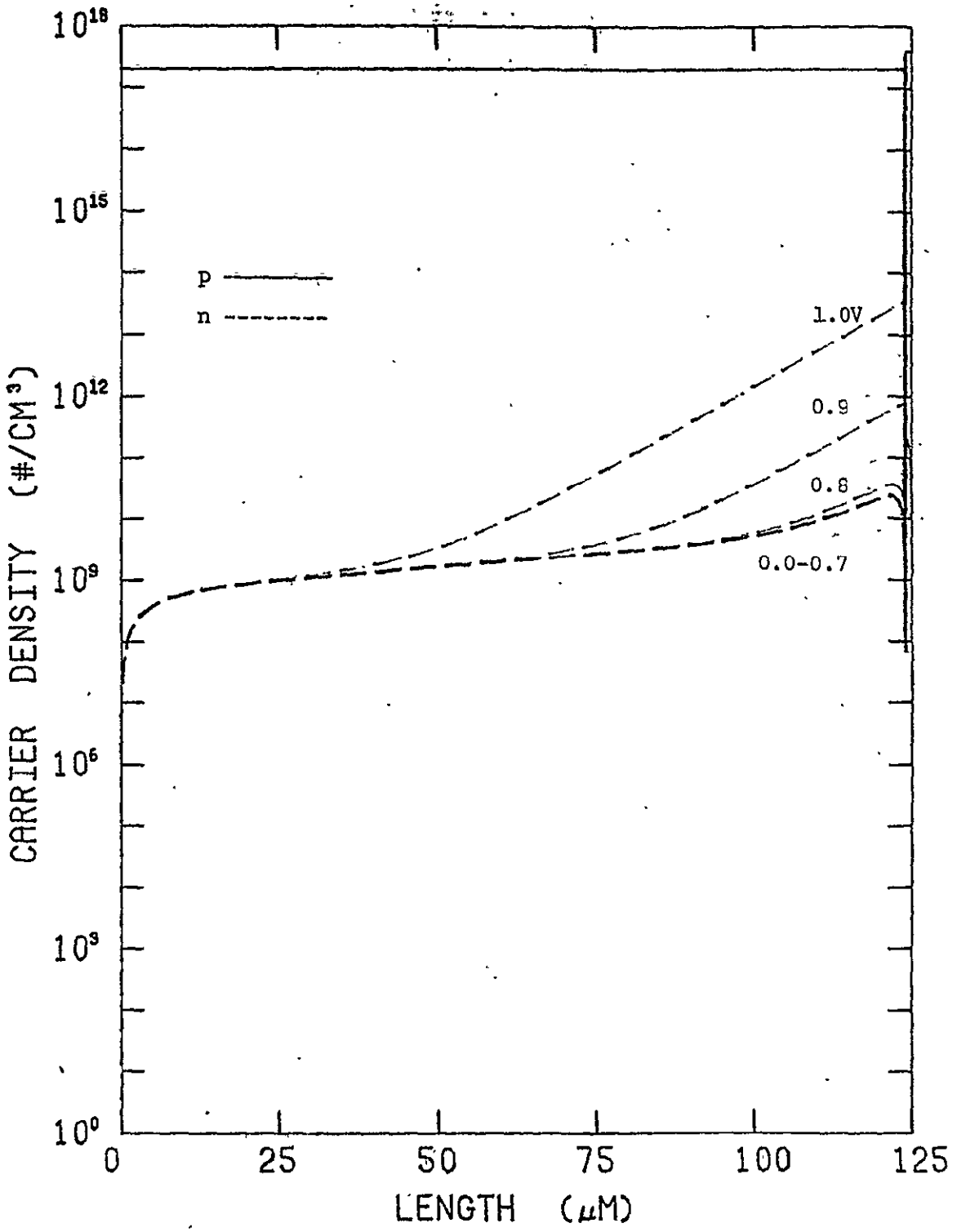


Figure 5.10 Electron and hole concentrations across cell 2

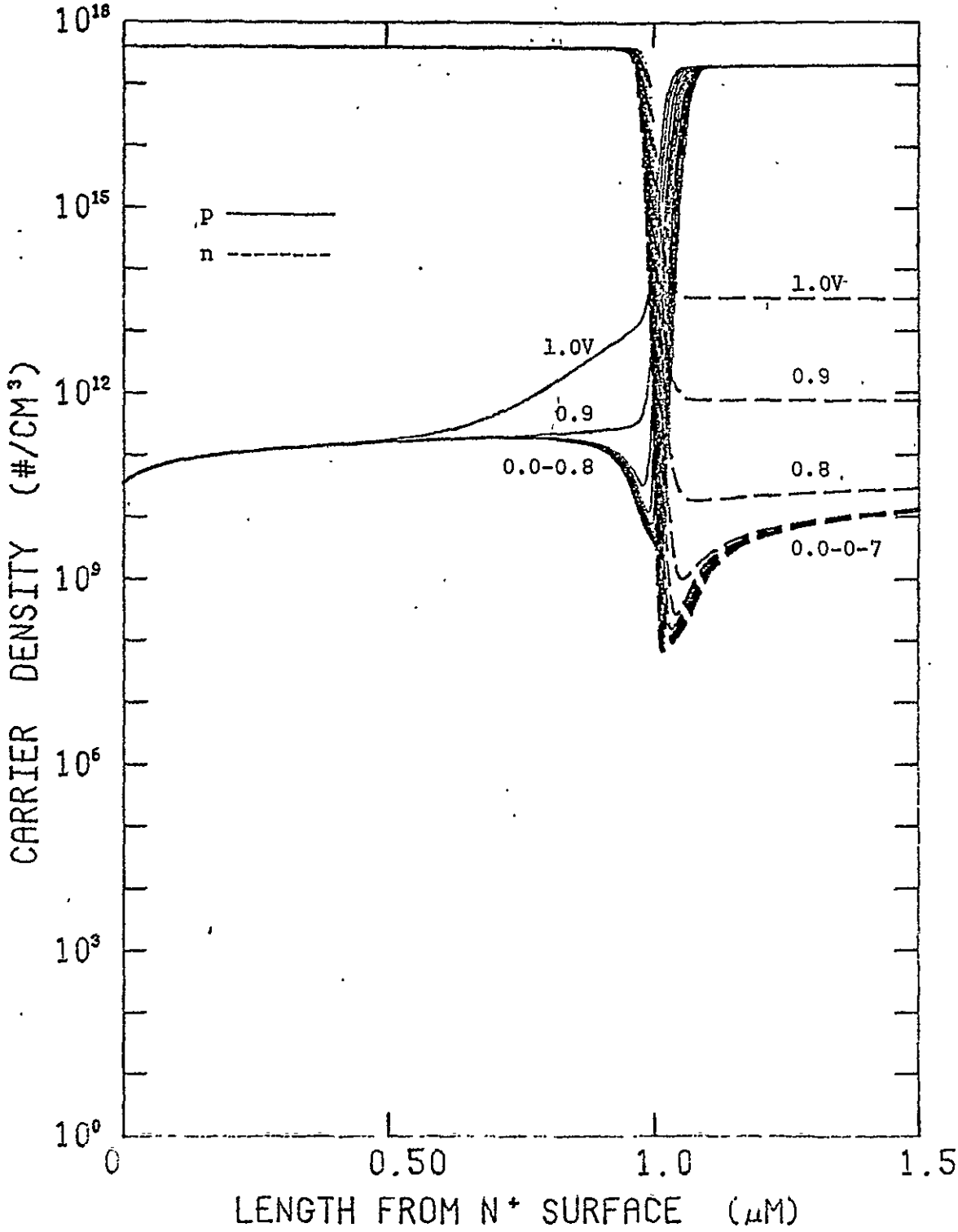


Figure 5.11 Electron and hole concentrations near the surface of cell 2

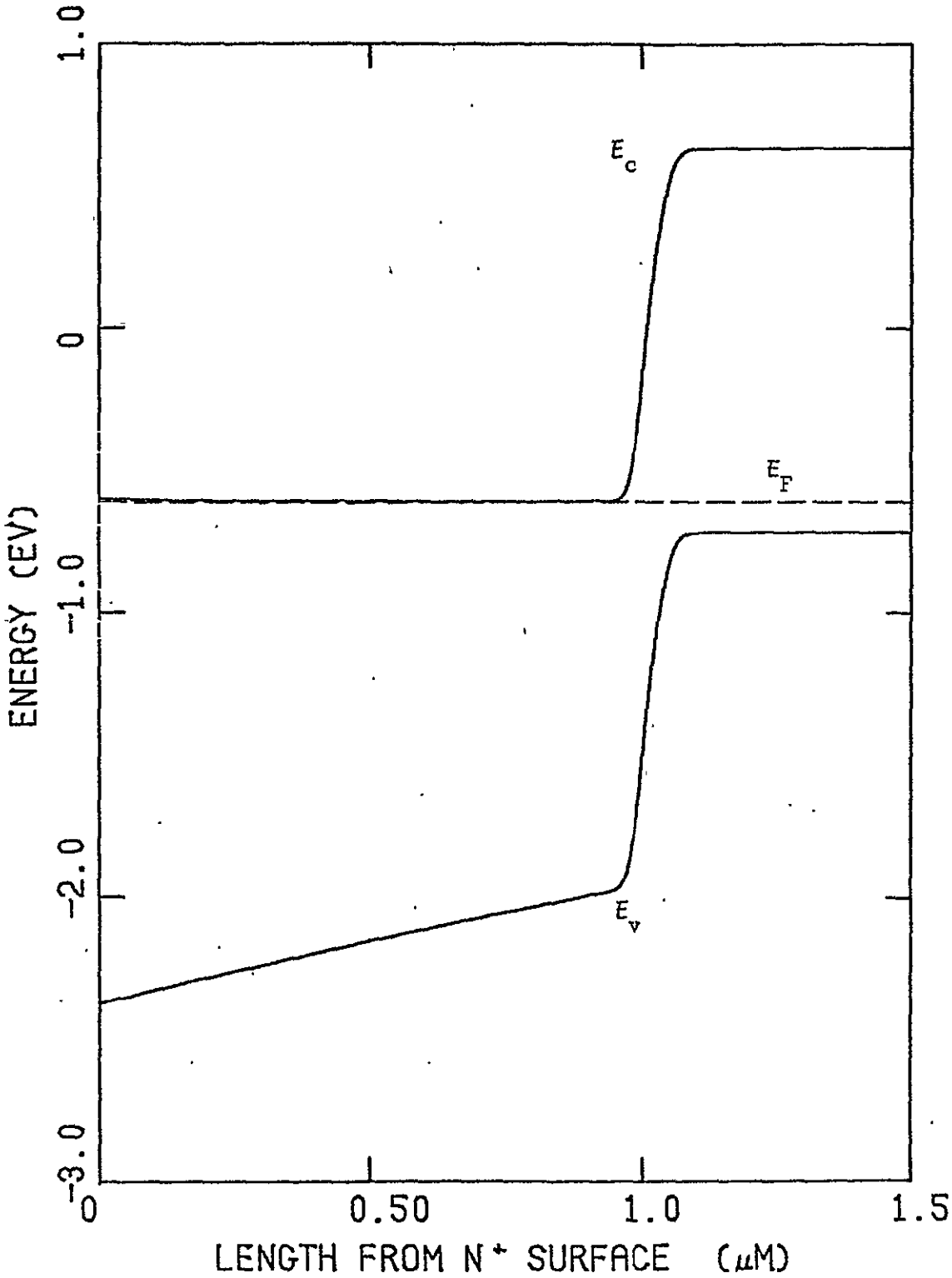


Figure 5.12 Electron energy band diagram for cell 2

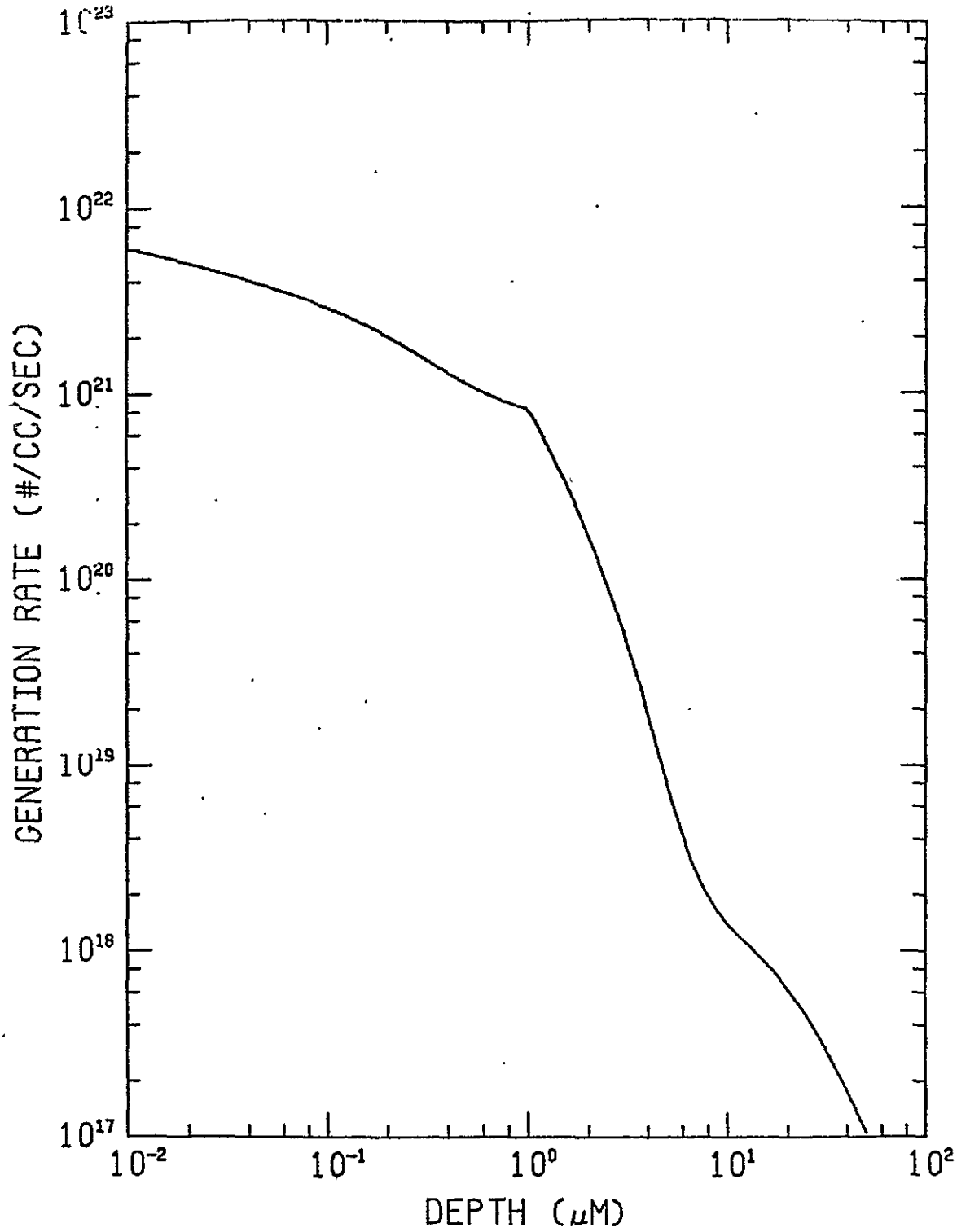


Figure 5.13 Optical generation rate profile of cell 2

Cell 3, however, has a linearly graded region from 100% AlAs at the surface to 0% AlAs at a depth of 1 μM, so that the direct-indirect transition occurs at about 0.6 μM below the surface. Figure 5.14 shows the pronounced change in the built-in potential at the point of transition, while the composition grading itself is linear. The corresponding energy band diagram and carrier concentrations for cell 3 are shown in Figures 5.15 through 5.17.

The generation rate profile of cell 6, shown in Figure 5.18 graphically illustrates the improved control over carrier generation rate distribution made possible by composition variation (see Section 2.4). This device consists of an AlAs layer on GaAs. The surface layer acts as a window to separate the high recombination rate at the surface from the high generation rate region below the heterojunction. The improved collection efficiency is responsible for making cell 6 the most efficient solar cell structure of the seven examined so far.

The relative performance of five of the most significant cells is depicted in Figures 5.19 through 5.22 with no correction for ohmic contact area. Although cell 2 has the largest short circuit current, cell 6 has the largest open circuit voltage and the highest peak efficiency. The main advantage of cell 6 over cell 2 is the greater concentration of carrier generation within the depletion region (compare Figures 5.13 and 5.18). The built-in field due to band gap grading in cell 2 fails to collect carriers efficiently enough to compensate for the fact that the maximum carrier generation rate occurs at the surface. Thus, cell 6 has a peak efficiency of 19.19% while cell 2 has a peak efficiency of only 17.92%.

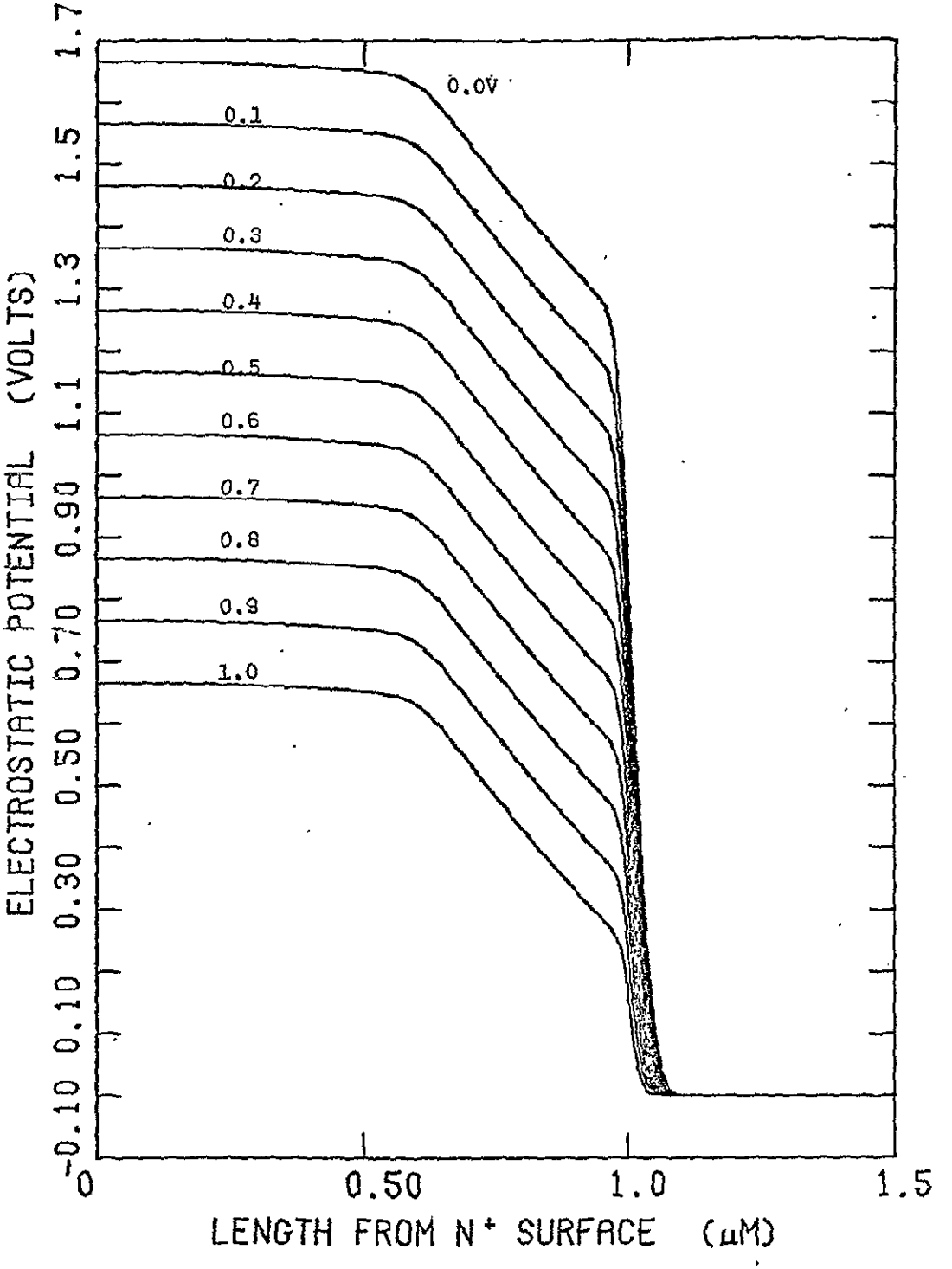


Figure 5.14 Electrostatic potential near the surface of cell 3

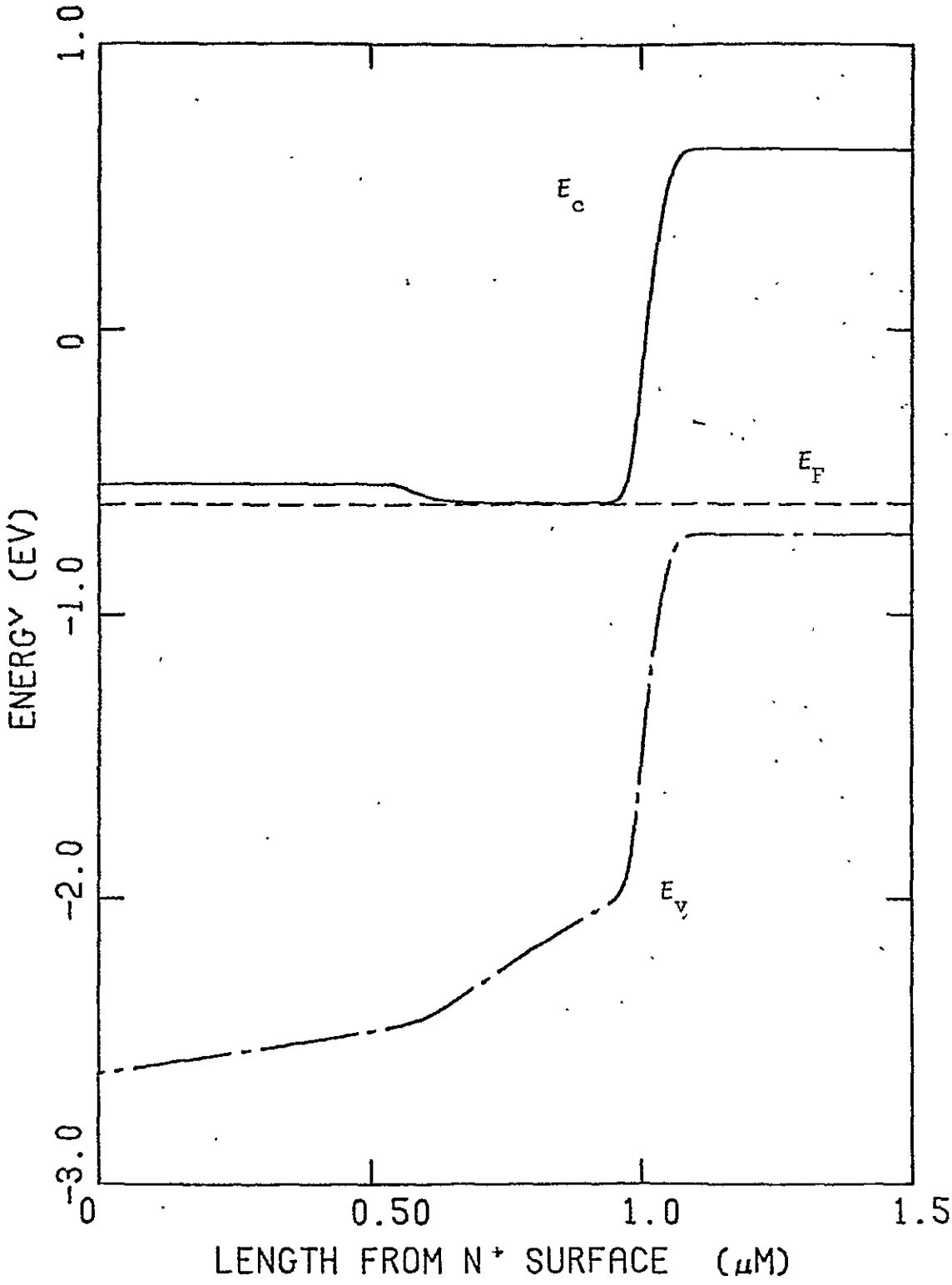


Figure 5.15 Electron energy band diagram for cell 3.

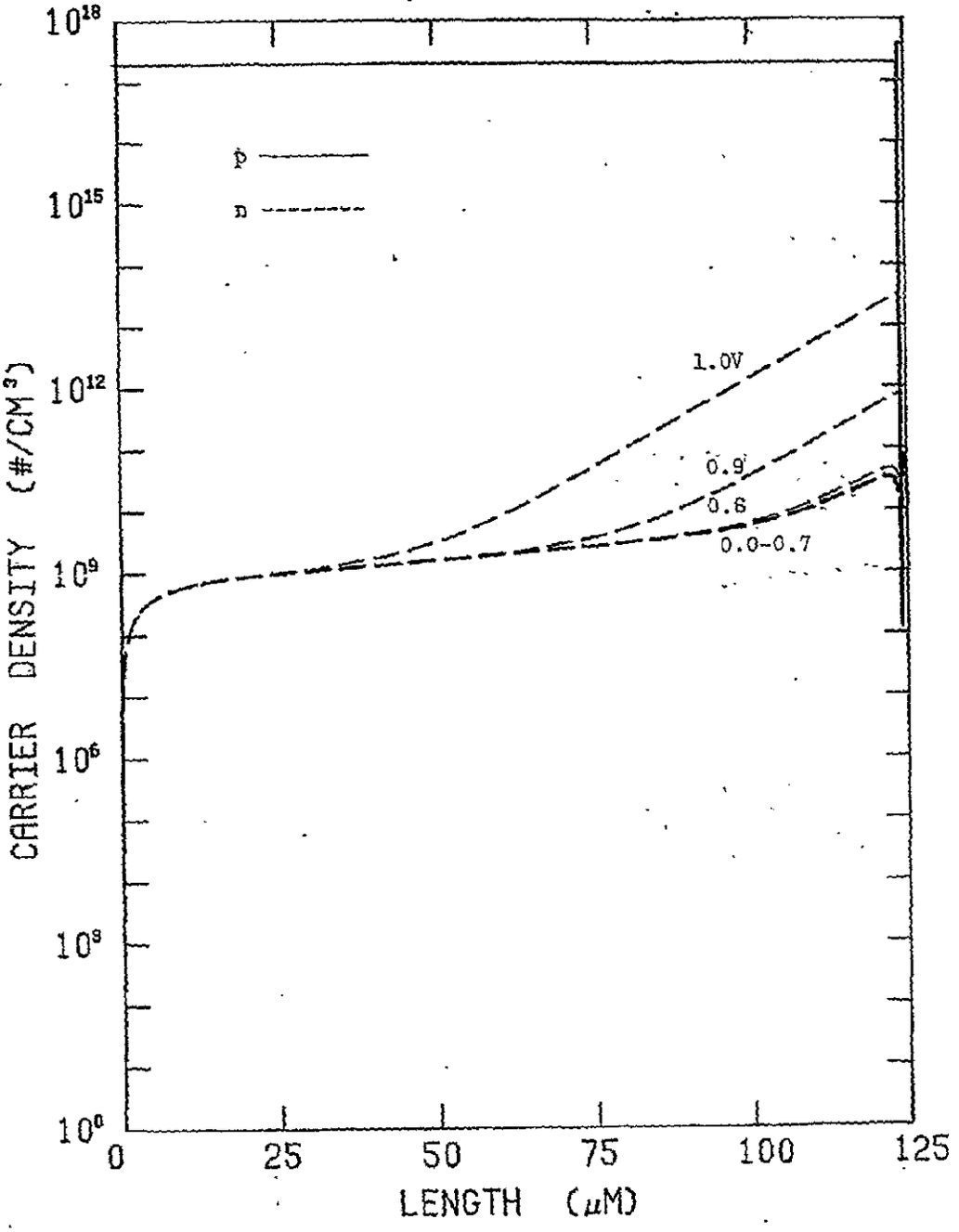


Figure 5.16 Electron and hole concentrations across cell 3

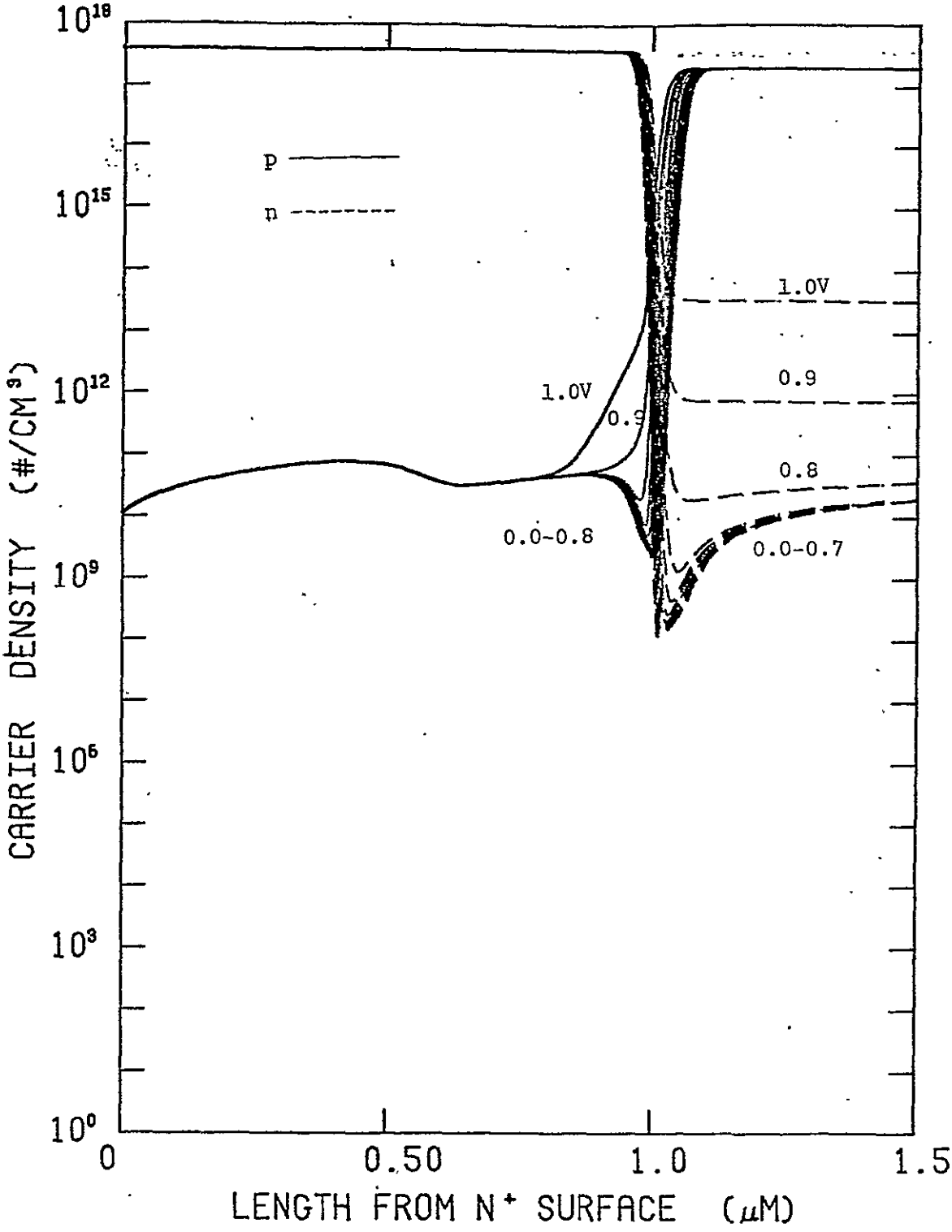


Figure 5.17 Electron and hole concentrations near the surface of cell 3

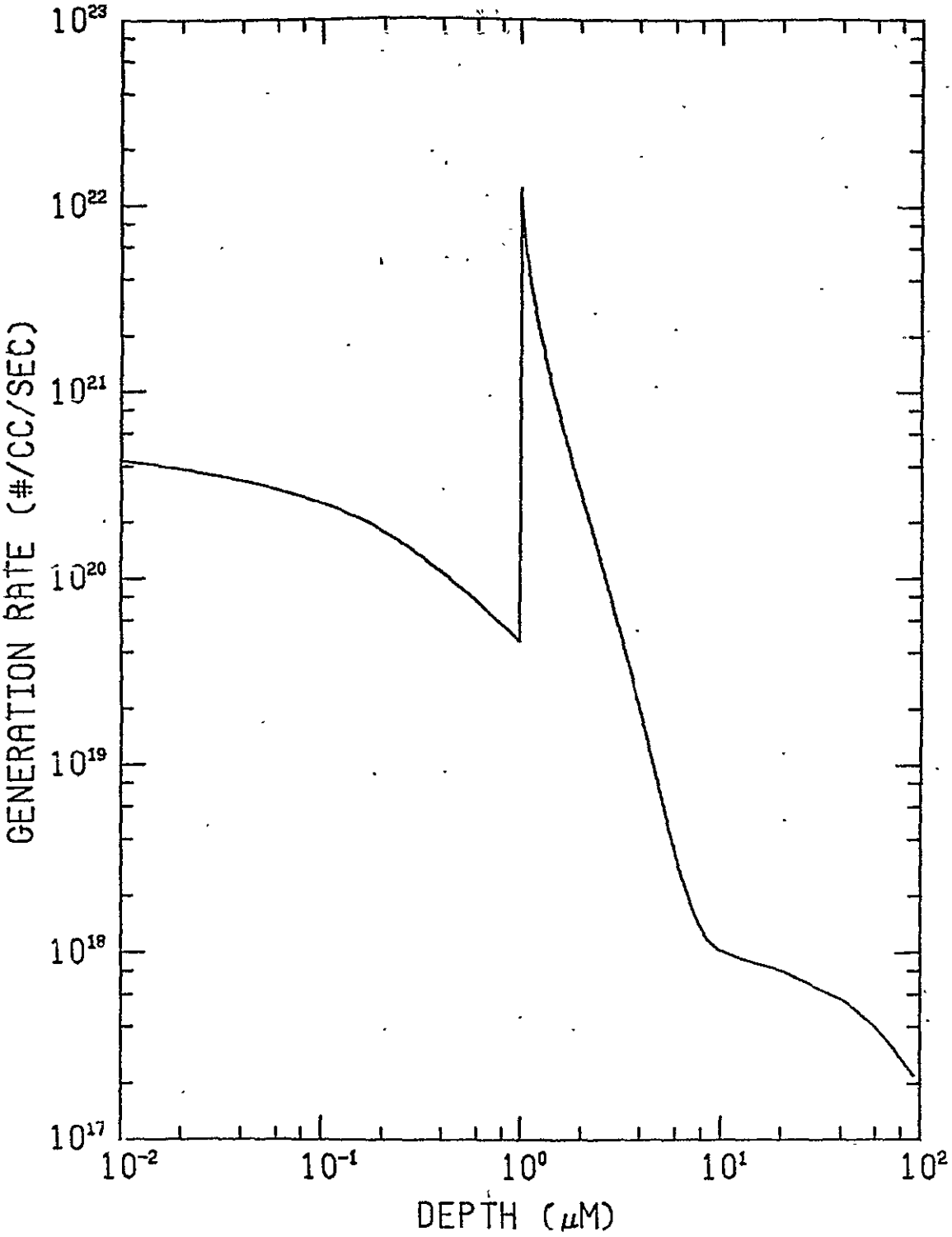


Figure 5.18 Optical generation rate profile for cell 6

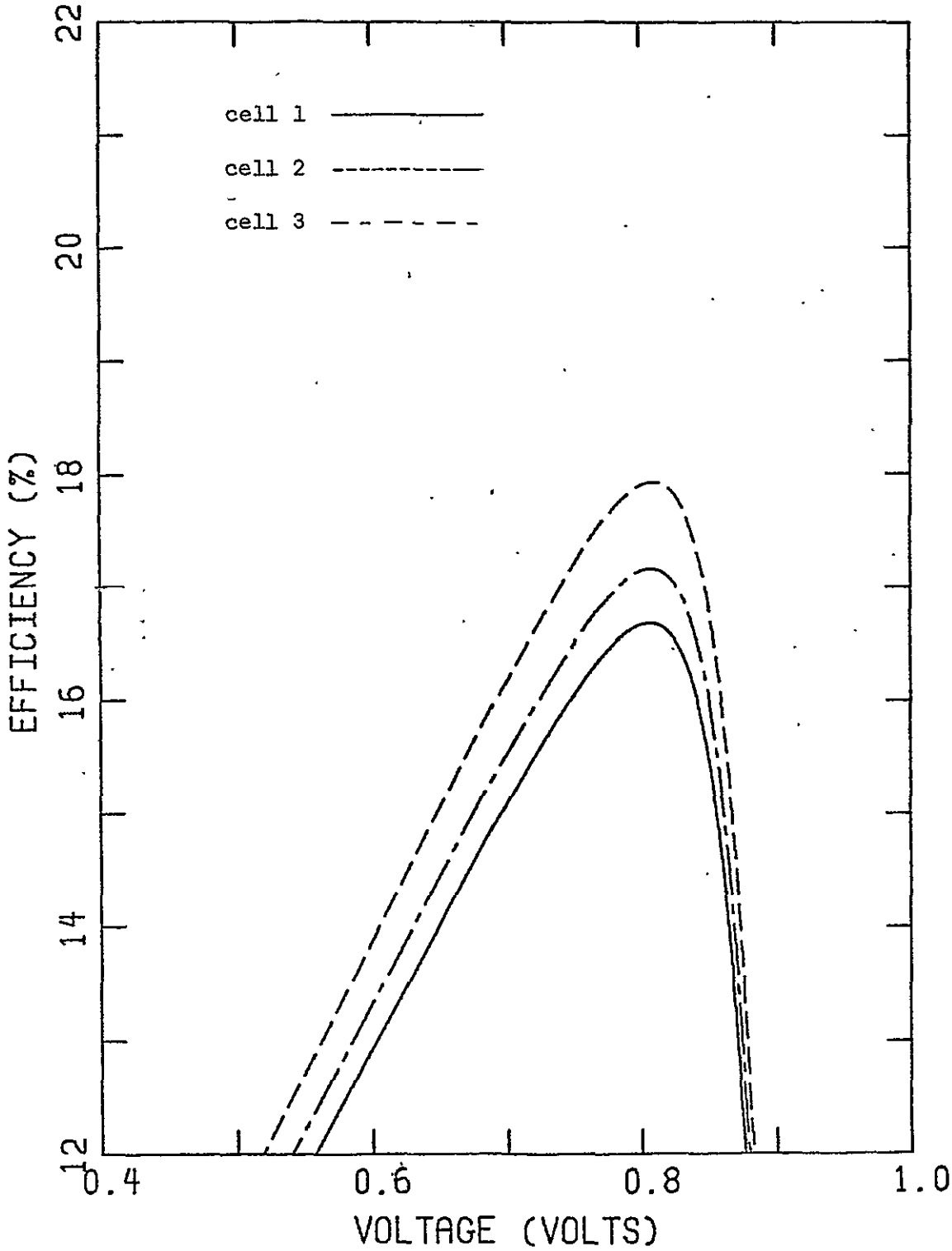


Figure 5.19 Efficiency characteristics for cells 1, 2 and 3

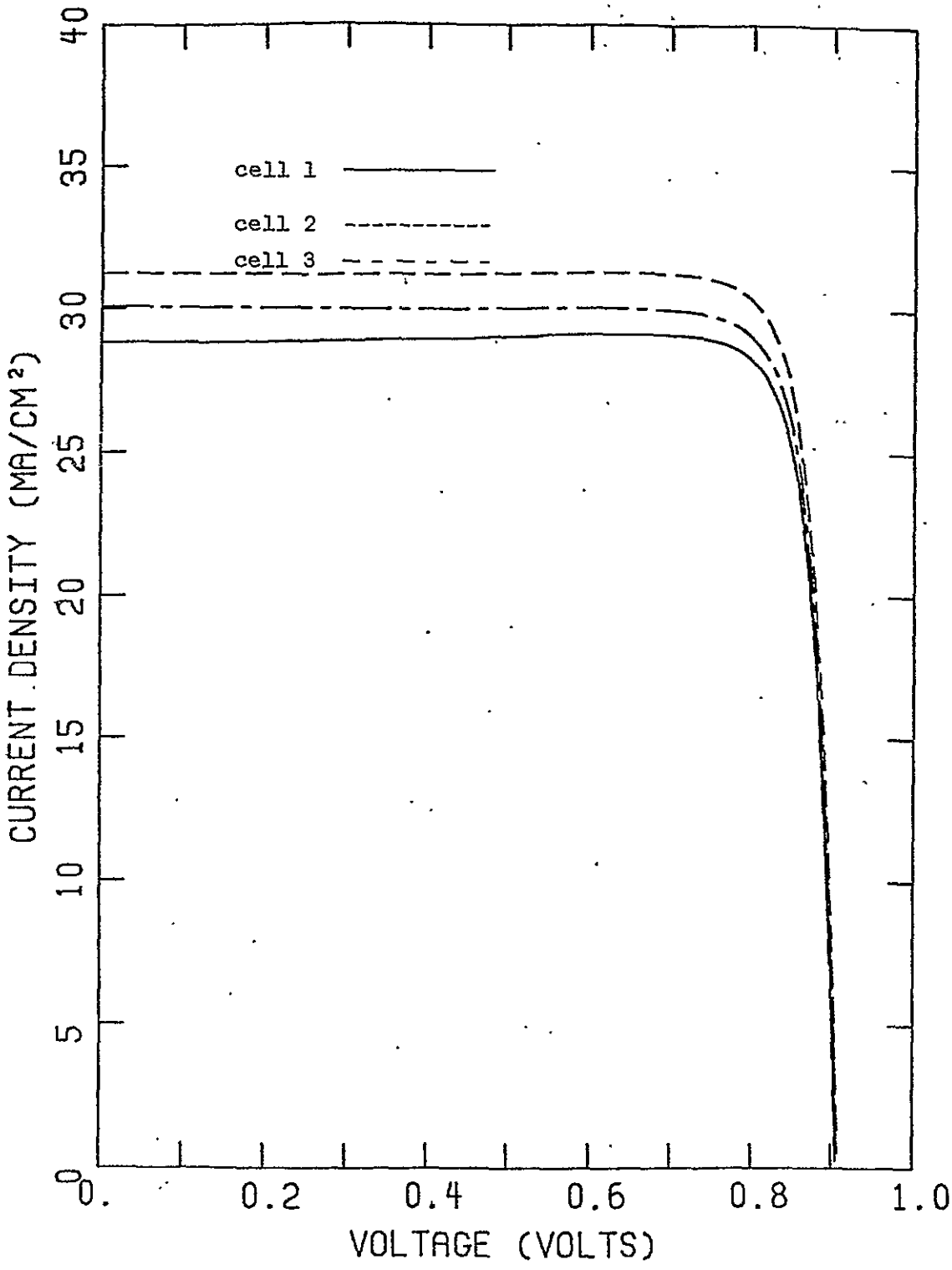


Figure 5.20 Current density vs. voltage characteristics for cell 1, 2 and 3

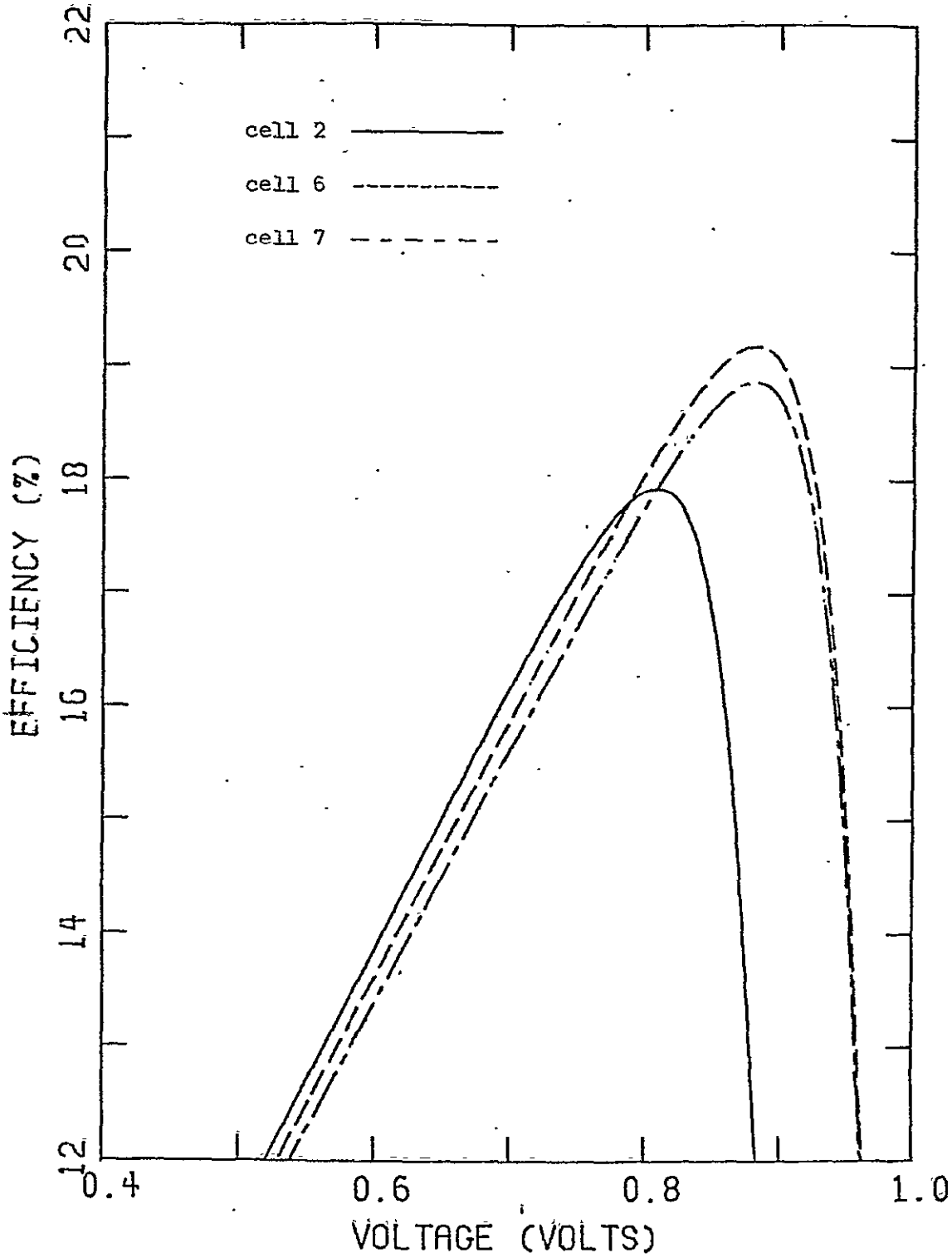


Figure 5.21 Efficiency characteristics for cells 2, 6 and 7

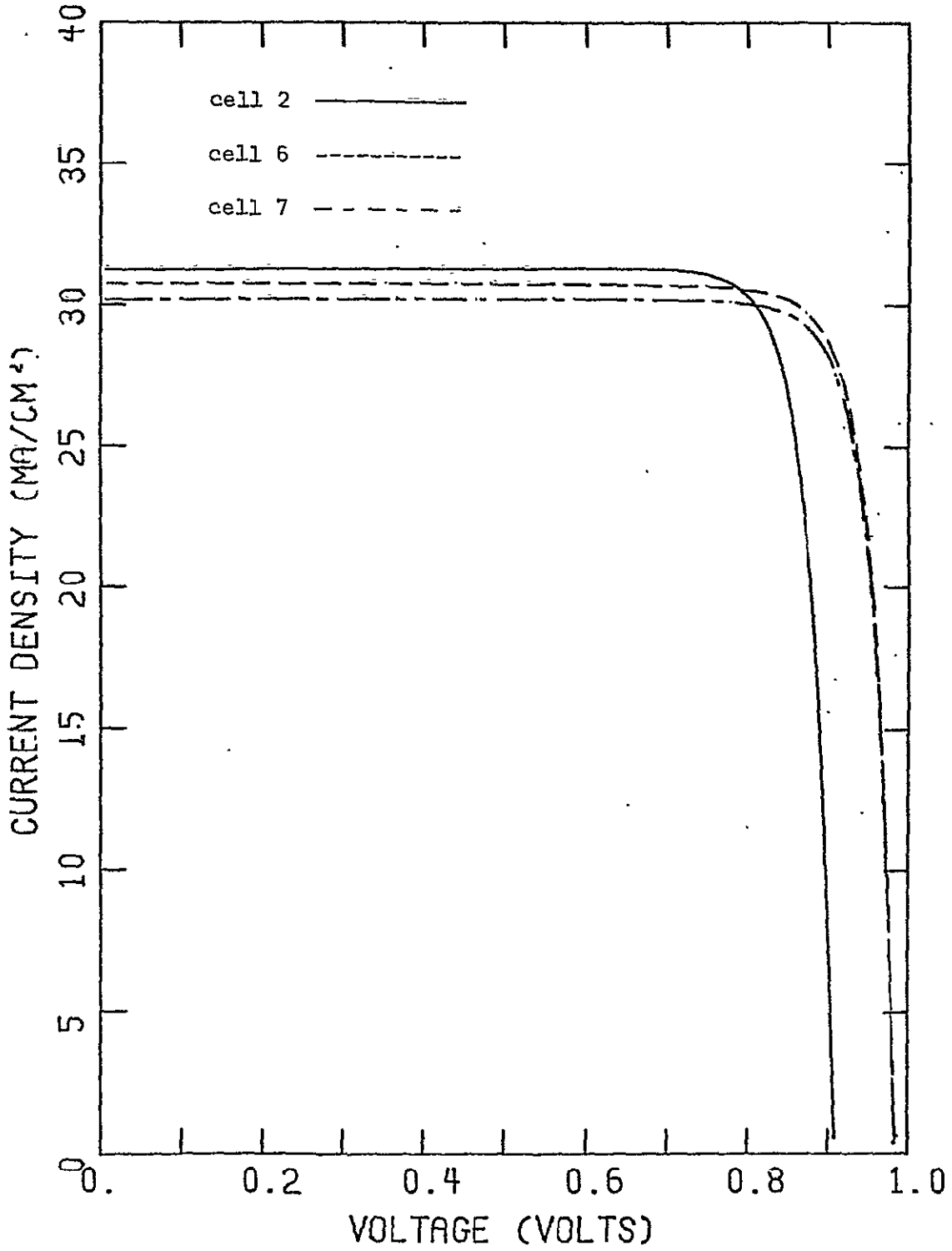


Figure 5.22 Current density vs. voltage characteristics for cells 2, 6 and 7

Although the performance data referred to so far is useful for the comparison of cells that have been analyzed by the computer, some correction for contact area must be made before a realistic estimate of practical efficiency can be made. Table 5.1 summarizes the significant performance parameters of the 7 cells analyzed up to the present time. The only correction for contact area appears in the last column of Table 5.1, where the idealized efficiency has been multiplied by a factor of 0.87 to correct for an assumed 13% metal contact coverage. Naturally, such a first order correction fails to allow for the fact that a given contact geometry does not alter the J vs. V characteristics of different devices in the same way. Also this simple correction factor does not account for the sheet resistance of the surface layer with a finger contact geometry. A more accurate correction for contact area and series sheet resistance can be expected in future analyses.

Figure 5.23 compares the results of an analysis by Hutchby [26] of several devices having linear composition grading, with the analysis of similar devices (cells 1, 2, and 3) by the variable composition solar cell analysis program. The device parameters of cells 1, 2, and 3 closely match those of the upper curve (see Sec. 5:2) in Hutchby's data and it is apparent that while the computer predicts slightly lower efficiency at each value of composition, the general dependence of efficiency on surface composition appears to be the same in both analyses.

Table 5.1 Solar cell performance parameters

| Device # | Open Circuit Voltage (Volts) | Short Circuit Current ($mA/cm^2$) | Fill Factor | Peak Efficiency (%) | Peak Efficiency (%) (13% Contact Coverage) |
|---|---|---|---|---|---|
| 1 | .906 | 28.89 | .862 | 16.68 | 14.51 |
| 2 | .909 | 31.25 | .854 | 17.92 | 15.59 |
| 3 | .907 | 30.10 | .850 | 17.16 | 14.93 |
| 4 | .898 | 21.85 | .843 | 12.24 | 10.65 |
| 5 | .928 | 29.09 | .921 | 18.39 | 16.00 |
| 6 | .984 | 30.77 | .857 | 19.19 | 16.70 |
| 7 | .985 | 30.22 | .858 | 18.87 | 16.42 |

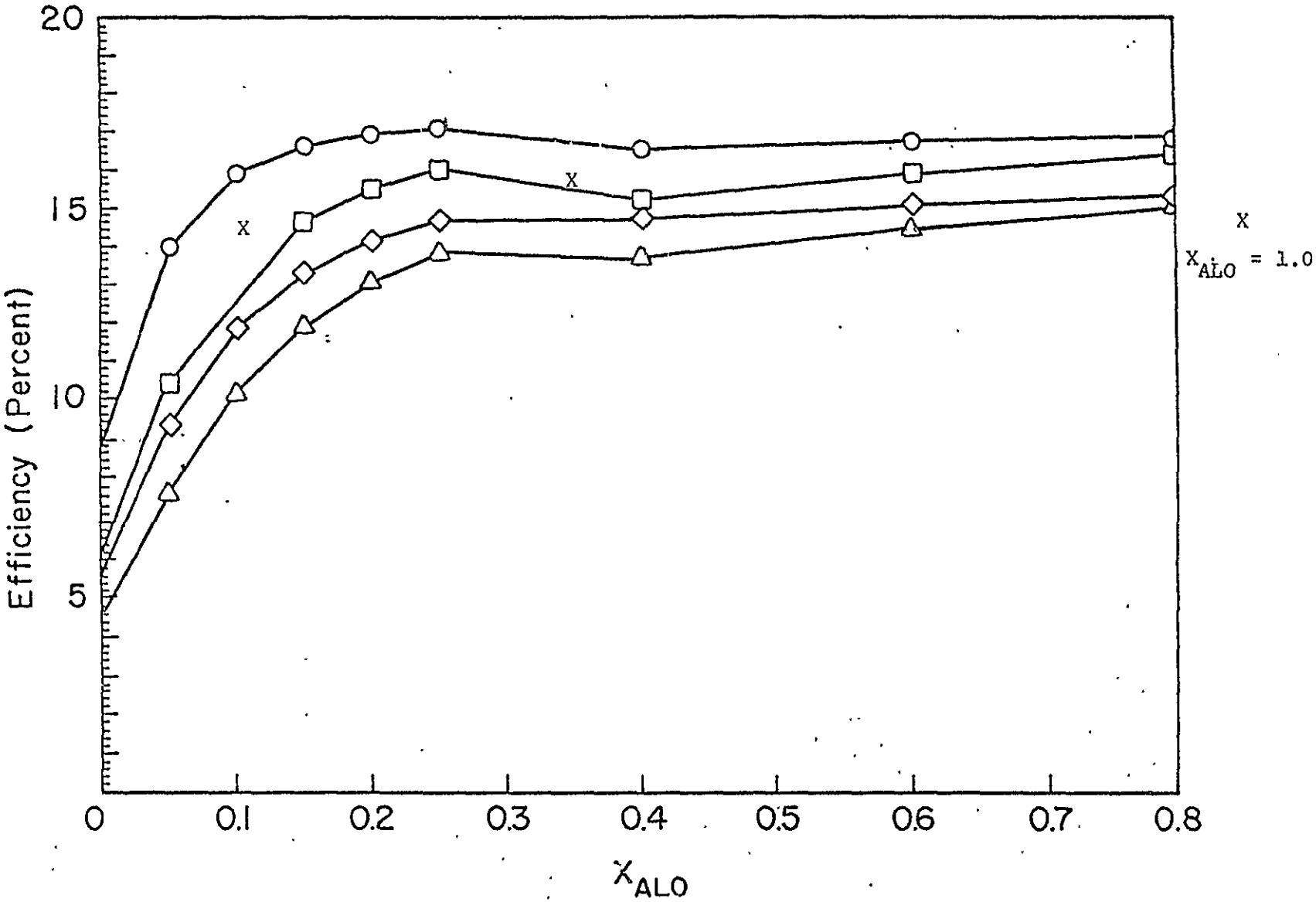


Figure 5.23 Efficiency vs. surface mole fraction of AlAs, $X_{ALO}$, at the surface. ○:S=1x10$^5$ cm/sec. $L_{po}$=2.1 μm; □:S=1x10$^6$ cm/sec, $L_{po}$=2.1μm; ◇:S=1x10$^5$ cm/sec, $L_{po}$=0.52 μm; △:S=1x10$^6$ cm/sec, $L_{po}$=0.52 μm [22]. X:cells 1,2 and 3 with characteristics comparable to ○.

## 6. Summary

As the preceding results indicate, the variable composition solar cell analysis program predicts efficiencies that are in agreement with qualitative estimates of solar cell performance. The shift of peak optical carrier generation away from the surface to the junction depletion region, made possible by position-dependent composition, has led to the expected increase in efficiency over that of homogeneous solar cells.

Future work will include: 1) an examination of the possible advantages of placing the p-n junction above or below the termination of composition grading, 2) a search for an optimum composition profile and the corresponding doping profile, 3) improved modeling of the dependence of lifetime on position, and 4) an examination of solar cells using alloys other than $Al_xGa_{1-x}As$. It is hoped that the analysis of various materials and structures will lead to a better understanding of the processes controlling variable composition solar cell performance.

## References


1. M. Wolf, "Limitations and possibilities for improvement of photovoltaic solar energy converters," Proc. IRE, vol 48, 1960, p. 1246.

2. J. J. Wysocki and P. Rappaport, "Effect of temperature on photovoltaic solar energy conversion", J. Appl. Phys., vol 31, 1960, p. 571.

3. Y. Marfaing and J. Chevallier, "Photovoltaic Effects in Graded Bandgap Structures", IEEE Trans. on ED, vol. ED-18, 1971, p.465.

4. P. M. Emtage, "Electrical Conductivity and the Photovoltaic Effect in Semiconductors with Position-Dependent Band Gaps", J. Appl. Phys., vol. 33, 1962, p. 1950.

5. H. K. Gummel, "A Self-Consistent Iterative Scheme for One-Dimensional Steady-State Transistor Calculations", IEEE Trans. on ED, ED-11, 455 (1964).

6. A. DeMari, "Accurate Numerical Steady-State and Transient One-Dimensional Solutions of Semiconductor Devices", Unpub. Ph.D. Thesis, California Institute of Technology, 1967.

7. C. M. Lee, R. J. Lomax, and G. I. Haddad, IEEE Trans. on MTT, MTT-22, 160 (1974).

8. E. D. Graham and J. R. Hauser, "Effects of Base Doping and Width on the J-V Characteristics of the $n^+$-n-$p^+$ Structure", Solid-State Elec., 15, 303 (1972).

9. P. M. Dunbar and J. R. Hauser, "A Theoretical Analysis of the Current-Voltage Characteristics of Solar Cells," Annual Report on NASA Grant NGR 34-002-195, August 1975.

10. J. M. Woodall and H. J. Hovel, "High-Efficiency $Ga_{1-x}Al_xAs$-GaAs Solar Cells", Appl. Phys. Lett. vol 21, 1972, p. 379.

11. H. J. Hovel and J. M. Woodall, "$Ga_{1-x}Al_xAs$-GaAs P-P-N Heterojunction Solar Cells", J. Electrochem. Soc., Vol 120, 1973, p. 1246.

12. J. W. Harrison, "Gallium Arsenide Technology", vol. I, Research Triangle Institute, Technical Report AFAL-TR-72-312, vol. I, January 1973.

13. Y. M. Yim, "Direct and Indirect Optical Energy Gaps of AlAs," Journal of Applied Physics, vol. 42, June 1971.

14. M. R. Lorenz, R. Chicotka, G. D. Pettit, and P. J. Dean, Solid State Communications, vol. 8, 1970.

References (continued)

15. A. Onton, Extended Abstracts, Inter. Conf. Phys. of Semiconductors, 10th, Cambridge, August, 1970 (unpublished).

16. H. C. Casey, Jr., D. D. Sell, and K. W. Wecht, "Concentration Dependence of the Absorption Coefficient for n- and p-type GaAs between 1.3 and 1.6 eV", Journal of Applied Physics, vol. 46, January, 1975.

17. A. Onton, M. R. Lorenz and J. M. Woodall, Bull. Am. Phys. Soc., vol. 16, p. 371, 1971.

18. H. C. Casey, Jr., and M. B. Pannish, Journal of Applied Physics, vol. 40, p. 4910 (1969).

19. J. J. Loferski, "Theoretical Considerations Governing the Choice of the Optimum Semiconductor for Photovoltaic Solar Energy Conversion," Journal of Applied Physics, vol. 7, pp. 777-784, July, 1956.

20. J. W. Harrison and J. R. Hauser, "Theoretical Calculations of Electron Mobility in Ternary III-V Compounds," Journal of Applied Physics, vol. 47, January, 1976.

21. E. M. Conwell, High Field Transport in Semiconductors, Academic Press, New York, 1967.

22. M. Neuberger, Handbook of Electronic Materials, vol. 2, III-V Semiconducting Compounds, Plenum Press, New York, 1971.

23. Obtained from a Monte Carlo calculation made by J. R. Hauser.

24. R. Tsu, L. L. Chaing, G. A. Sai-Halasz, and L. Esaki, "Effects of Quantum States on a Photocurrent in a Superlattice, "Physical Review Letters, vol. 34, June 1975.

25. NASA, 1971, Solar Electromagnetic Radiation, NASA Document, NASA SP 8005.

26. J. A. Hutchby, "High Efficiency Graded Band Gap $Al_xGa_{1-x}As$-GaAs Solar Cell;" Applied Physics Letters, vol. 26, p. 457, 1975.

27. J. A. Hutchby and R. L. Fudurich, "Theoretical Analysis of $Al_xGa_{1-x}As$-GaAs Graded Band-Gap Solar Cell," submitted for publication to the Journal of Applied Physics.

28. J. A. Hutchby and R. L. Fudurich, "Theoretical Optimization and Parametric Study of n-on-p $Al_xGa_{1-x}As$-GaAs Graded Band-Gap Solar Cells," submitted for publication to the Journal of Applied Physics.

29. D. L. Rode, "How much Al in the AlGaAs-GaAs Laser?", Journal of Applied Physics, vol. 45, September, (1974).